DMD Fast Forward. Published on June 4, 2020 as DOI: 10.1124/dmd.120.000039
This article has not been copyedited and formatted. The final version may differ from this version.

DMD-AR-2020-000039R1

Impact of Microbiome on Hepatic Metabolizing Enzymes and Transporters in Mice during Pregnancy

Lyrialle W. Han, Lu Wang[†], Yuanyuan Shi[†], Joseph L. Dempsey, Olesya V. Pershutkina, Moumita Dutta, Theo K. Bammler, Julia Y. Cui, and Qingcheng Mao[*]

LWH, QM: Department of Pharmaceutics, School of Pharmacy, University of Washington, Seattle, Washington, USA

LW, JLD, MD, TKB, JYC: Department of Environmental and Occupational Health Sciences, School of Public Health, University of Washington, Seattle, Washington, USA

YS: Department of Medicinal Chemistry, School of Pharmacy, University of Washington, Seattle, Washington, USA

OVP: Department of Comparative Medicine, School of Medicine, University of Washington, Seattle, Washington, USA

[†]Authors of equal contribution

[*]Corresponding author

DMD-AR-2020-000039R1

Running Title: Microbiome and Pregnancy on Hepatic Enzymes and Transporters

Corresponding author:

Qingcheng Mao, PhD
Department of Pharmaceutics
School of Pharmacy
University of Washington
H272F, Health Science Building
Box 357610
1959 NE Pacific St.
Seattle, WA 98195-7610
Email: qmao@uw.edu
Tel: +1 (206) 685-0355

Number of text pages: 44

Number of tables: 5

Number of figures: 10

Number of references: 54

Number of words in Abstract: 244

Number of words in Introduction: 743

Number of words in Discussion: 1500

Abbreviations: DPG, drug processing gene; CV, conventional; GF, germ-free; CVNP, conventional non-pregnant; CVP, conventional pregnant; GFNP, germ-free non-pregnant; GFP, germ-free pregnant; LC-MS/MS; liquid chromatography tandem mass spectrometry; GR, glucocorticoid receptor; PXR/Nrli2, pregnane X receptor; FXR/Nr1h4, farnesoid X receptor; Abc, ATP-binding cassette transporter family; Slc, solute carrier family; solute carrier organic anion (Slco) transporter family; Cyp, cytochrome P450; Ugt, UDP-glucuronosyltransferases;

Sult, sulfotransferases; Gst, glutathione *S*-transferases; HAS, human serum albumin; BSA, bovine serum albumin; DCA, deoxycholic acid; CA, cholic acid; CDCA, chenodeoxycholic acid; UDCA, ursodeoxycholic acid; α/β-MCA, alpha/beta-murine cholic acid; HDCA, hyodeoxycholic acid; LCA, lithocholic acid; MDCA, murideoxycholic acid; ω-MCA, omega-muricholic acid; Bsep, bile salt efflux pump; P-gp/Abcb1/Mdr, P-glycoprotein; Mrp3/Abcc3, multidrug resistance associated protein 3; Bcrp/Abcg2, breast cancer resistance protein; Oct2/Slc22a2, organic cation transporter 2; Oat2/Slc22a7, organic anion transporter 2; Oatp/Slco, organic anion transporting polypeptide; qRT-PCR, quantitative reverse transcription-polymerase chain reaction; DMETs, drug metabolizing enzymes and transporters.

DMD Fast Forward. Published on June 4, 2020 as DOI: 10.1124/dmd.120.000039
This article has not been copyedited and formatted. The final version may differ from this version.

Abstract

The microbiome and pregnancy are known to alter drug disposition, yet the interplay of the two physiological factors on the expression and/or activity of drug metabolizing enzymes and transporters (DMETs) is unknown. This study investigated the effects of microbiome on host hepatic DMETs in mice during pregnancy by comparing four groups of conventional (CV) and germ-free (GF) female mice and pregnancy status, namely CV non-pregnant (CVNP), GF non-pregnant (GFNP), CV pregnant (CVP), and GF pregnant (GFP) mice. Transcriptomic and targeted proteomics of hepatic DMETs were profiled using multi-omics. Plasma bile acid and steroid hormone levels were quantified by LC-MS/MS. CYP3A activities were measured by mouse liver microsome incubations. The trend of pregnancy-induced changes in the expression or activity of hepatic DMETs in CV and GF mice was similar; however, the magnitude of change was noticeably different. For certain DMETs, pregnancy status had paradoxical effects on mRNA and protein expression in both CV and GF mice. For instance, the mRNA levels of *Cyp3a11*, the murine homolog of human *CYP3A4*, were decreased by 1.7-fold and 3.3-fold by pregnancy in CV and GF mice, respectively; however, the protein levels of CYP3A11 were increased similarly ~2-fold by pregnancy in both CV and GF mice. Microsome incubations revealed a marked induction of CYP3A activity by pregnancy that was 10-fold greater in CV mice than that in GF mice. This is the first study to show that the microbiome can alter the expression and/or activity of hepatic DMETs in pregnancy.

Significance Statement: We demonstrated for the first time that microbiome and pregnancy can interplay to alter the expression and/or activity of hepatic drug metabolizing enzymes and transporters. While the trend of pregnancy-induced changes in the expression or activity of hepatic drug metabolizing enzymes and transporters in conventional and germ-free mice was similar, the magnitude of change was noticeably different.

DMD Fast Forward. Published on June 4, 2020 as DOI: 10.1124/dmd.120.000039
This article has not been copyedited and formatted. The final version may differ from this version.

Introduction

Drug safety in pregnant women is a critical issue for drug development and regulatory agencies due to observed changes in efficacy and toxicity of medications during pregnancy (Beigi *et al.*, 2016; FDA, 2018). Understanding how drug disposition is changed in pregnant women is therefore of utmost importance (see below). However, there remain gaps in knowledge of other factors that can affect drug disposition in this vulnerable population. The impact of the microbiome on drug disposition could be one such example (Sharma *et al.*, 2019).

Pregnancy changes the maternal body in numerous ways to accommodate the developing fetus. Increased total body volume, decreased plasma albumin, increased cardiac output and renal glomerular filtration rate, and altered expression or activity of drug metabolizing enzymes and transporters (DMETs) profoundly alter drug disposition in pregnant women versus non-pregnant women or men (Helldén and Madadi, 2013; Isoherranen and Thummel, 2013; Pariente *et al.*, 2016; Tasnif *et al.*, 2016). Previous studies have shown increased activity of CYP3A4, CYP2D6, and CYP2C9, and decreased activity of CYP2C19 and CYP1A2, by using respective probe substrates prescribed to women during pregnancy (Feghali *et al.*, 2015). Drug transporters also could have dynamic activity or mRNA expression changes during pregnancy. For example, the activity of P-glycoprotein (P-gp) and organic cation transporter 2 (OCT2) in the kidney appears to be induced during human pregnancy, whereas mRNA expression of multidrug resistance protein 3 (Mrp3/Abcc3) in the mouse liver is down-regulated by pregnancy (Isoherranen and Thummel, 2013; Shuster *et al.*, 2013). Pregnancy-related hormones such as progesterone, estradiol, and cortisol which are ligands of nuclear receptors such as glucocorticoid receptor (GR) and pregnane X receptor (PXR) have been proposed to mediate induction of DMETs during pregnancy (Kliewer *et al.*, 1998; Dussault *et al.*, 2003; Papacleovoulou *et al.*,

2011). Therefore, a mechanistic understanding of the changes in expression or activity of DMETs during pregnancy will help optimize the dosing regimens of drugs for improved efficacy and safety for both the mother and her fetus.

The microbiome is often referred to as the second human genome due to the abundance and diversity of bacteria. The microbiome can change drug disposition and toxicity profiles by directly metabolizing and inactivating compounds (Spanogiannopoulos *et al.*, 2016). Indirectly, gut bacteria can alter drug disposition by changing the expression or activity of host DMETs (Spanogiannopoulos *et al.*, 2016). It has been proposed that the predominant mechanism by which bacteria modulate DMET expression is by the modification of secondary bile acids (Claus *et al.*, 2011; Klaassen and Cui, 2015). Primary bile acids are synthesized in the liver from cholesterol and subsequently transported into the bile duct by efflux transporters, such as the bile salt export pump (BSEP). The bile duct leads primary bile acids into the duodenum where intestinal bacteria deconjugate, dehydroxylate, and epimerize them into secondary bile acids. Intestinal bacteria such as *Clostridia* from Firmicutes phylum express the enzymes (e.g. hydroxysteroid dehydrogenase and 7-dehydratase) necessary for these biotransformation reactions (Ridlon *et al.*, 2006). The primary bile acids cholic acid (CA) and chenodeoxycholic acid (CDCA), as well as secondary bile acid deoxycholic acid (DCA) and their taurine conjugated forms have been shown to activate farnesoid X receptor (FXR), which regulates bile acid production (Wang *et al.*, 1999; Kong *et al.*, 2012). Lithocholic acid (LCA) has been shown to activate PXR (Staudinger *et al.*, 2001), which in turn up-regulates the expression of certain CYPs. In mice, it has been demonstrated that the primary muricholic acids are antagonists of FXR, thus the lack of transformation of primary bile acids into secondary bile acids in GF mice would result in accumulation of FXR antagonists (primary bile acids) and reduction of PXR

agonists (secondary bile acids); ultimately, this decreases FXR and PXR signaling in the intestine and the liver (Klaassen and Cui, 2015; Wahlström *et al.*, 2017). Recently, it was shown that the maternal gut microbiome shifts as pregnancy progresses in humans, with an increase in the abundance of *Actinobacteria* and *Proteobacteria*, which could alter bile acid profiles and DMET expression and/or activity (Nuriel-Ohayon *et al.*, 2016).

Although both pregnancy and the microbiome individually have a profound impact on drug disposition, no studies to date have investigated their combined effects. The objective of this study was to explore the combined effects of pregnancy and the microbiome on the expression and/or activity of hepatic DMETs using CV and GF pregnant mice. We hypothesize that the magnitude and direction of changes in expression and/or activity reflect the combined effects of pregnancy and the microbiome.

Materials and Methods

Chemicals

Liquid chromatography-mass spectrometry grade methanol, water, and acetonitrile were purchased from Fisher Scientific (Fair Lawn, NJ). Steroid hormone standards and deuterated internal standards for bile acids (lithocholic acid, deoxycholic acid, cholic acid, glycochenodeoxycholic acid, and glycocholic acid) were purchased from Cerilliant Corporation (Round Rock, TX) and Steraloids Inc. (Newport, RI). All other chemicals were obtained from Thermo Fisher Scientific (Rockford, IL) unless stated otherwise.

Animal studies

DMD Fast Forward. Published on June 4, 2020 as DOI: 10.1124/dmd.120.000039
This article has not been copyedited and formatted. The final version may differ from this version.

Conventional C57BL/6J mice (JAX stock #000664) from The Jackson Laboratory (Bar Habor, ME) were habituated for one week at our own animal facility prior to experiments. Germ-free C57BL/6 colony were originated from mice purchased from the National Gnotobiotic Rodent Resource Center of the University of North Carolina at Chapel Hill. The conventional (CV) and germ-free (GF) mice have the same genetic background. All animals were cared for in accordance with the Guide for the Care and Use of Laboratory Animals published by the National Research Council. The animal protocol was approved by the Institutional Animal Care and Use Committee of the University of Washington (protocol# 4035-04). Germ-free mice were housed at the University of Washington Gnotobiotic Animal facility in isolators.

Both CV and GF mice were maintained on 12-h light/dark cycles, and the same autoclaved Breeder Chow #5021 (LabDiet, St. Louis, MO), autoclaved non-acidified water, and autoclaved Enrich-N'Pure bedding (The Andersons Inc., Maumee, OH) were provided *ad libitum*. CV female mice at 8 weeks of age were mated with CV male mice overnight, and male mice were promptly separated from female mice in the morning. The day with the overnight housing was defined as gestation day (gd) 0. Due to difficulties in achieving pregnancies in GF mice, GF female mice of 11-15 weeks of age were mated with male mice for 72 h prior to separation from GF male mice. Day 2 after introduction of male mice to the cage was assumed to be gd 0. For the purpose of tissue collection, all pregnant CV or GF mice were kept individually in separate cages during the period of gestation after mating. All pregnant mouse tissues were collected on gd 15, which was previously shown to be the optimal time point to observe peak levels of gene expression changes (Shuster *et al.*, 2013). Non-pregnant female mice of similar ages (8-15 weeks) were housed exactly the same as pregnant mice as described above. On the day of tissue collection, pregnant or non-pregnant female mice were anesthetized with isoflurane, and blood

DMD Fast Forward. Published on June 4, 2020 as DOI: 10.1124/dmd.120.000039
This article has not been copyedited and formatted. The final version may differ from this version.

was collected via cardiac puncture and immediately centrifuged (1,500 × *g* for 10 min at 4°C) to isolate plasma. Tissues (e.g. liver) were removed, washed in cold saline, and immediately snap-frozen in liquid N_2. In total, plasma samples and tissues from 6 CVNP, 5 CVP, 6 GFNP, and 5 GFP mice were collected. All samples were then stored at -80°C until analysis.

RNA-seq analysis

Total RNA was extracted from liver tissues using Qiagen RNeasy Mini Kit (Qiagen, Hilden, Germany) following the manufacturer's instructions. The concentration of total RNA was determined by using a Synergy HTX Multi-mode Plate Reader (BioTek, Winooski, VT) at 260 nm. Paired end RNA sequencing (2 × 150 bp) was performed by Novogene Bioinformatics Technology Co., Ltd. (Sacramento, CA) using the Illumina NovaSeq 6000 with average 20 million reads. The library was prepared using NEBNext® Ultra™ RNA Library Prep Kit from Illumina®. We aligned reads to the mouse GRCm38.p6 transcriptome (Gencode release M19) using the *Salmon* aligner (v0.11.3) (Patro *et al.*, 2015) and then the transcript-level counts were imported into R and summarized at the gene level using the Bioconductor tximport package (v1.10.1) (Soneson *et al.*, 2015). Data was subsequently filtered to remove genes that had consistently low expression levels to improve the signal-to-noise ratio using filterByExpr function in the edgeR package (v3.24.3), implemented in R (v3.5.1). After filtering, 18849 genes remained. Differential gene expression analysis between groups was performed using the edgeR package with a negative binomial generalized linear model (GLM), and quasi-likelihood F-tests for a given contrast (Robinson *et al.*, 2009; Chen *et al.*, 2016). A false discovery rate (FDR) of 10% was selected to limit the number of false positives (Benjamini and Hochberg, 1995). RNA-seq data presented in this study were deposited in the National Center for Biotechnology Information Gene Expression Omnibus data repository under accession number GSE143391.

DMD Fast Forward. Published on June 4, 2020 as DOI: 10.1124/dmd.120.000039
This article has not been copyedited and formatted. The final version may differ from this version.

Quantitative real-time PCR

Quantitative real-time polymerase chain reaction (qRT-PCR) was performed to determine the mRNA levels of selected genes, as previously described, to validate RNA sequencing data (Shuster *et al.*, 2013). Aliquots from the same total RNA samples used for RNA-seq analysis were transcribed to cDNAs using random primers from High-Capacity cDNA Reverse Transcription Kit (Applied Biosystems, Foster City, CA). We selected 4 enzyme genes coding (*Cyp2b13, Cyp2c50, Cyp3a16, and Sult4a1*) and 2 transporter genes (*Abcc3* and *Slco1a4*) for validation. The genes were selected based on the large magnitude of change in mRNA abundance observed from RNA-seq analysis. The cDNAs were amplified using SsoAdvanced Universal SYBR Green Supermix and the Bio-Rad CFX384 Real-Time PCR Detection System (Hercules, CA). PCR primers were synthesized by Integrated DNA Technologies (Coralville, IA). *Gapdh* was used as a housekeeping gene for normalization of the gene expression data.

Targeted proteomic analysis of hepatic DMETs by LC-MS/MS

Quantification of relative protein abundance of major DMETs in the liver tissues of CV and GF mice was done by quantitative LC-MS/MS proteomic analysis using methods previously described (Bhatt and Prasad, 2018; Liao *et al.*, 2018; Prasad *et al.*, 2018). For CYP enzymes, changes in protein levels of CYP2C37, CYP2C50, CYP2C54, CYP2D22, CYP2D40, CYP3A11, CYP3A16, and CYP3A41 were quantified. For transporters, changes in protein levels of ABCB11, ABCB1A, ABCB1B, ABCC3, ABCG2, SLC22A2, SLC22A7, SLCO1A1, and SLCO1A4 were determined. We used the same procedures for protein isolation and digestion as previously published (Prasad *et al.*, 2018). Briefly, approximately 50 mg of frozen liver tissue

DMD Fast Forward. Published on June 4, 2020 as DOI: 10.1124/dmd.120.000039
This article has not been copyedited and formatted. The final version may differ from this version.

per mouse was homogenized in 2 ml of permeabilization buffer (the permeabilization and protease inhibitor solution mix) using dounce hand homogenizer. All steps were carried out on ice to minimize protein degradation. The resulting liver homogenate was shaken for 30 min at 4°C then centrifuged at 16,000 × *g* for 15 min. The resulting supernatant was aliquoted for protein quantification via BCA analysis and diluted to 2 mg/ml prior to trypsin digestion. To 80 µl of post-treatment supernatant, 30 µl of ammonium bicarbonate buffer (100 mM, pH 7.8), 10 µl of human serum albumin (HSA), 20 µl of bovine serum albumin (BSA), and 10 µl of dithiothreitol (DTT) were added and incubated at 95°C for 10 min. After cooling, 20 µl of iodoacetamide (500 mM) was added to incubate at room temperature for 30 min in the dark. Then, ice-cold methanol (0.5 ml), chloroform (0.1ml), and water (0.4ml) was added to desalt the samples. After centrifugation at 16,000 × *g* for 5 min at 4°C, the pellet was washed with ice-cold methanol (0.5 ml) and centrifuged at 8000 × *g* for 5 min at 4°C.Trypsin (20 µl, 1:10 trypsin: protein ratio (w/w)) was added and incubated for 16 h at 37°C while shaking at 300 rpm. The reaction was quenched with dry ice and internal standards were added. The relative levels of protein abundance of CYP enzymes and transporter were quantified using surrogate peptides for respective CYP enzymes or transporters as standards (Supplemental Table S1). Chromatographic and mass spectrometric conditions were the same as previously described (Prasad *et al.*, 2018). Previous studies (Bhatt and Prasad, 2018) found that it was necessary to perform various normalization steps in order to minimize batch-to-batch and sample-to-sample variation. Therefore, bovine serum albumin (BSA) and a stable-isotope labeled heavy peptide cocktail were added as normalization controls. The quality of peptide signal was verified by plotting the correlation between two or more peptide fragments or transitions derived from different samples with the same total protein concentration. Ion suppression was assessed with multiple peptides

DMD Fast Forward. Published on June 4, 2020 as DOI: 10.1124/dmd.120.000039
This article has not been copyedited and formatted. The final version may differ from this version.

from the same protein. This approach measures whether the variability in peak responses reflects the biological variability. In addition, by adding BSA, an exogenous protein, into the homogenized sample before protein denaturation, the sample loss during subsequent processing steps was addressed. Moreover, the use of heavy isotope-labeled peptides as internal standard provided adjustment for possible matrix effects and sample concentration changes due to evaporation and nonspecific binding to the vials. Relative protein abundance of each enzyme or transporter was calculated by taking the average signal for all peptides that passed linearity test for each enzyme or transporter in each individual liver sample and dividing it by the average signal of the corresponding heavy isotope-labeled peptide. The ratio was subsequently normalized to BSA and the group mean (pool of all samples) of each surrogate peptide. The resulting ratio-of-ratio (ROR) estimates reflect relative protein abundance of each individual enzyme or transporter. The samples used for proteomic analysis were essentially the same as those used for RNA-seq analysis or activity assay (see below) except that the number of samples used for proteomic analysis in the CVP and GFNP groups was 4 instead of 5 or 6, due to a lack of sufficient tissue homogenates.

Liver microsome isolation and activity assay

Liver microsomes were prepared from individual mouse livers, as previously described (Paine *et al.*, 1997; Shuster *et al.*, 2014). All steps were carried out at 4°C to minimize protein degradation. Approximately 750 mg of frozen mouse liver tissue was homogenized in 2 ml homogenization buffer (50 mM KPi buffer containing 0.25 M sucrose and 1 mM EDTA) using Omni Bead Ruptor Homogenizer (Omni International, Kennesaw, GA). The homogenate was then centrifuged for 30 min at 15,000 × *g*, and the resulting supernatant was centrifuged for 70 min at 120,000 × *g*. The pellet containing microsomes was washed once with the buffer (10 mM

KPi, 0.1 mM KCl, 1 mM EDTA, pH 7.4) before a final centrifugation for 70 min at 120,000 × *g*. The final pellet was resuspended in 1 ml of the storage buffer (50 mM KPi, 0.25 M sucrose, 10 mM EDTA, pH 7.4) and stored in 200 µl aliquots at -80°C until analysis. Microsomal protein concentration was determined using the Pierce BCA Protein Assay Kit (Thermo Scientific, Rockford, IL).

CYP3A activities in individual liver microsomal preparations were determined using the Promega P450-Glo Screening Kit (Promega Corporation, Madison, WI) according to the manufacturer's instruction. Briefly, liver microsomes (7 µg per reaction) from CV and GF mice were pre-incubated with 3 µM luminogenic P450-Glo Luciferin-IPA for 10 min at 37°C. In the case of the inhibition assay, ketoconazole was added to the reaction mixture to a final concentration of 5 µM as previously described (Perloff et al., 1999). Then, NADPH regeneration system was added to the mixture to initiate reaction. Total reaction volume was 75 µl. After incubation of 10 min at 37°C, reaction was stopped by the addition of equal volume of the luciferin detection reagent at room temperature and let the mixture sit for 20 min. Cyp3a-mediated reaction results in generation of a luciferin product, which was measured by a Glomax 96 Microplate Luminometer (Promega Corporation, Madison, WI). Light signal detected reflects the magnitude of Cyp3a activity. Both the substrate concentration and time of incubation were optimized to fall within the linear range of human CYP3A activity, as reported by Promega and described in its instruction. Control incubations using recombinant CYP3A4 microsomes were also performed in parallel as positive control. Incubations were done in triplicates and repeated once. The same assay kit has previously been used to measure mouse Cyp3a activity (Lee *et al.*, 2013; Selwyn *et al.*, 2015; Li *et al.*, 2017).

Quantification of plasma bile acids and steroid hormones

DMD Fast Forward. Published on June 4, 2020 as DOI: 10.1124/dmd.120.000039
This article has not been copyedited and formatted. The final version may differ from this version.

Bile acids were extracted from mouse plasma as previously described (Alnouti *et al.*, 2008). Briefly, 50 µl of plasma sample was mixed with 10 µl of internal standard solution (20 µg/ml d4-G-CDCA, 10 µg/ml d4-G-CDCA in 50% MeOH) and vortexed well. Protein was precipitated by adding 500 µl ice-cold methanol. The mixture was centrifuged at 12,000 × *g* for 10 min at 4°C. The resulting supernatant was kept in a new tube and the pellet was put through the same steps. The resulting supernatant was combined with the previous one, dried under vacuum (30°C) and reconstitute in100 µl of 1:1 methanol/water (v/v). The suspension was centrifuged again at 12,000 × *g* for 10 min at 4°C and 50 µl was subjected into the ultra-performance liquid chromatography coupled with mass spectrometry in tandem (UPLC-MS/MS) for analysis. Chromatographic conditions and instrument settings were the same as described (Alnouti *et al.*, 2008) with modifications. Samples were eluted using mobile phases (A) consisted of 20% acetonitrile and 10 mmol/L ammonium acetate in aqueous solutions and (B) consisted of 80% acetonitrile and 10 mmol/L ammonium acetate in aqueous solutions, at a flow rate of 0.400 ml/min. Five µl of each sample was injected on column for analysis using negative ionization mode.

Primary bile acids cholic acid (CA), chenodeoxycholic acid (CDCA), ursodeoxycholic acid (UDCA), alpha/beta-murine cholic acid (α/βMCA), and their respective taurine conjugates (TCA, T-CDCA, TUDCA, T-α/βMCA) as well as secondary bile acids deoxycholic acid (DCA), hyodeoxycholic acid (HDCA), lithocholic acid (LCA), murideoxycholic acid (MDCA), omega-muricholic acid (ωMCA), and their respective taurine conjugates (T-ωMCA, T-DCA, T-HDCA, and T-LCA) were quantified. Calibrator and different quality control (QCs) samples were prepared by adding the appropriate amount of the different standard stock solutions and were extracted using the similar sample preparation procedure described above.

DMD Fast Forward. Published on June 4, 2020 as DOI: 10.1124/dmd.120.000039
This article has not been copyedited and formatted. The final version may differ from this version.

Steroid hormones were extracted from mouse plasma as previously described (Basit *et al.*, 2018). Briefly, 200 µl of methanol containing an internal standard cocktail (10 µg/ml estrone-d4, 10 µg/ml cortisol-d4, 10 µg/ml 11-deoxycortisol-d5, 10 µg/ml DHEA-d5, 10 µg/ml progesterone-d9, 10 µg/ml 17OH-progesterone-d8, and 10 µg/ml 17OH-pregnenolone-d3) was added to 50 µl of plasma samples, and the mixture was mixed vigorously for 1 min followed by a centrifugation at 3,500 × *g* for 10 min at 4°C. The supernatant was moved to a new micro centrifuge tube and dried down under N_2. Samples were reconstituted in 50% methanol and analyzed by LC-MS/MS using the same instrument and conditions as described (Basit *et al.*, 2018).

Statistical analyses for plasma metabolite quantification and microsome activity

Data are presented as means ± SE (or SD) of independent samples from 4 – 6 different mice. Statistical significance of the difference between two groups was determined by the Wilcoxon T test, with $p < 0.05$ to be considered as significant. Data analyses were performed using R (v3.5.1 & v3.6.1) and GraphPad Prism (GraphPad Prism 5.01, La Jolla, CA).

Results

Validation of RNA-seq data by qRT-PCR

A direct comparison of the two approaches (RNA-seq and qRT-PCR) is shown in Fig. 1 for 6 selected genes (*Cyp3a16, Cyp2b13, Cyp2c50, Sult4a1, Abcc3, and Slco1a4*). Overall, gene expression levels determined by the two approaches showed the same pattern of pregnancy-induced changes in both CV and GF mice (up-regulation or down-regulation). More specifically, *Cyp2b13, Cyp2c50, Sult4a1, Abcc3,* and *Slco1a4* demonstrated down-regulation by both RNA-

DMD Fast Forward. Published on June 4, 2020 as DOI: 10.1124/dmd.120.000039
This article has not been copyedited and formatted. The final version may differ from this version.

seq and qRT-PCR analyses. As for *Cyp3a16,* down-regulation in GFNP group and up-regulation in CVNP, CVP, and GFP groups were observed. The consistency of these results established the accuracy and reliability of the more comprehensive RNA-seq analysis.

RNA-seq analysis of hepatic DMETs

To determine whether pregnancy and the microbiome interact to affect the expression of host hepatic DMETs, we performed RNA-seq analysis of liver tissues from CVNP (n = 6), CVP (n = 5), GFNP (n = 6), and GFP (n = 5) C57BL/6 mice. Specifically, we examined the mRNA expression profiles of genes important for xenobiotic, bile acid, and steroid hormone disposition, including phase I enzymes (cytochrome P450 (*Cyp*) enzymes), phase II enzymes (UDP-glucuronosyltransferases (*Ugt*), sulfotransferases (*Sult*), and glutathione *S*-transferases (*Gst*)), and transporters (ATP-binding cassette (*Abc*) transporters, solute carrier (*Slc*) transporters, and solute carrier organic anion (*Slco*) transporters). Differential changes in the expression of key DMETs by pregnancy in CV and GF mice are shown in Table 1. A complete list of DMETs as determined by RNA-seq analysis can be found in Supplemental Table S2.

There were no significant differences in the expression of DMETs between CVNP and GFNP mice, with either no change or slight trend of down-regulation for most of the DMETs listed in Table 1 in GFNP mice compared to CVNP mice. Comparing pregnant mice, we found the mRNA levels of two genes, *Cyp2b13 and Cyp2c38,* were higher, 5.3-fold (*FDR* < 0.001) and 3-fold (*FDR* = 0.013), respectively, in GFP mice compared to CVP mice (Table 1). The expression of other DMET genes was not significantly different between CVP and GFP mice (Table 1).

DMD Fast Forward. Published on June 4, 2020 as DOI: 10.1124/dmd.120.000039
This article has not been copyedited and formatted. The final version may differ from this version.

In both CV and GF mice, pregnancy induced significant changes in the expression of many DMETs in phase I (Fig. 2) and phase II (Fig. 3) enzymes, as well as transporters (Fig. 4), relative to non-pregnant mice. Pregnancy altered the expression of DMETs with an overall similar trend, but with different magnitudes of changes, in CV and GF mice. For example, pregnancy decreased the mRNA expression of *Cyp2c37, Cyp2c38, Cyp2c50* and *Cyp2c54* by 70% (*FDR* < 0.01), 60% (*FDR* < 0.01), 80% (*FDR* < 0.001) and 60% (*FDR* < 0.01), respectively, in CV mice, whereas in GF mice, no significant or much smaller changes by pregnancy were observed for the same genes (Table 1). Similarly, *Cyp2d40* was induced 3.9-fold (*FDR* < 0.001) and 5.4-fold (*FDR* < 0.001) by pregnancy, respectively, in CV and GF mice (Table 1 and Fig. 2). Among all the *Cyp* isoforms analyzed, CV and GF mice showed the most differences in the gene expressions of *Cyp3a* isoforms in response to pregnancy (Table 1 and Fig. 2). We observed a 70% down-regulation of *Cyp3a11* by pregnancy in GF mice (*FDR* = 0.005), but a non-significant down-regulation in CV mice by pregnancy. The mRNA levels of *Cyp3a16* were induced 20.6-fold (*FDR* < 0.001) by pregnancy in CV mice versus 128-fold (*FDR* < 0.001) in GF mice. Likewise, *Cyp3a41a* and *Cyp3a41b* were induced by pregnancy 4.8-fold and 74.2-fold (*FDR* < 0.05 and *FDR* < 0.001, respectively) in CV mice compared to 10.8-fold and 181.7-fold (*FDR* = 0.002 and *FDR* < 0.001, respectively) in GF mice. *Cyp3a44* was up-regulated by 14.3-fold (*FDR* < 0.001) by pregnancy in CV mice versus 30.5-fold (*FDR* < 0.001) in GF mice.

Of all phase II enzymes that were differentially expressed during pregnancy, we noted that the most significant changes induced by pregnancy were associated with *Sult3a2* and *Sult4a1* in both CV and GF mice. We observed a 53.9-fold (*FDR* < 0.001) induction by pregnancy in CV mice versus a 226.7-fold (*FDR* < 0.001) induction in GF mice for *Sult3a2*, and

DMD Fast Forward. Published on June 4, 2020 as DOI: 10.1124/dmd.120.000039
This article has not been copyedited and formatted. The final version may differ from this version.

a 287.7-fold (*FDR* < 0.001) induction in CV mice versus only a non-significant induction in GF mice for *Sult4a1* (Table 1 and Fig. 3).

For transporters, *Abcc3* and *Slco1a4* were down-regulated by pregnancy to a similar extent in CV and GF mice (Table 1 and Fig. 4). *Abcc3* was down-regulated by pregnancy by 70% (*FDR* < 0.05) and 90% (*FDR* < 0.001), respectively, in CV and GF mice. *Slco1a4* was decreased 60% by pregnancy in CV mice (*FDR* < 0.05), but non-significantly in GF mice. Pregnancy induced *Slc22a2* and *Slc22a7* by 561.5-fold (*FDR* < 0.001) and 3.1-fold (*FDR* = 0.004), respectively, in GF mice, versus 260.5-fold (*FDR* < 0.001) induction of *Slc22a2* and a non-significant induction of *Slc22a7* in CV mice (Table 1 and Fig. 4).

Quantification of relative protein abundance of selected hepatic DMETs by targeted proteomics

To investigate and compare how protein levels of hepatic DMETs were changed by pregnancy in CV and GF mice, we performed quantitative proteomics of selected hepatic DMETs in liver tissues. Due to the limited amount of isolated liver membrane proteins available, we performed targeted proteomics only on a set of selected DMETs. Selection of DMETs was based on *a priori* knowledge of their importance in overall xenobiotic disposition (Nelson *et al.*, 2004). Relative protein abundance of theses DMETs was quantified using LC-MS/MS-based proteomics and results are shown in Fig. 5 and Fig. 6.

Of the phase I enzymes, we opted to quantify mouse isoforms homologous to human CYP2C19 (CYP2C37, CYP2C50 and CYP2C54), human CYP2D6 (CYP2D22 and CYP2D40), and human CYP3A4 (CYP3A11, CYP3A16, CYP3A41A and CYP3A41B). Because there are no distinct methods to separate CYP3A41A and CYP3A41B, the results for these two enzymes

DMD Fast Forward. Published on June 4, 2020 as DOI: 10.1124/dmd.120.000039
This article has not been copyedited and formatted. The final version may differ from this version.

were combined as CYP3A41. Overall, the effects of pregnancy on protein expression profiles of these Cyp enzymes in CV and GF mice were notably different from the effects of pregnancy on respective mRNA expression profiles. Specifically, we found that pregnancy significantly increased the protein levels of CYP3A11 approximately 2-fold in both CV and GF mice (Fig. 5), whereas the mRNA levels of *Cyp3a11* were down-regulated by pregnancy in CV and GF mice (Fig. 2). There were no significant differences in the protein levels of CYP3A16 between CVNP and CVP or between GFNP and GFP; however, the protein level of CYP3A16 in CVP mice was significantly higher (~25%) than in GFP mice (0.95 ± 0.04 vs. 0.72 ± 0.03, $p < 0.05$) (Fig. 5). The effect of pregnancy on protein expression of CYP3A41 was similar to its effect on mRNA expression with a trend of higher abundance in pregnancy for both CV and GF mice; however, a statistically significant increase by pregnancy was observed only in CV mice (Fig. 5). No significant differences in the protein levels of CYP2C and CYP2D isoforms between CVNP and CVP or between GFNP and GFP were observed (Fig. 5). Like CYP3A16, the protein levels of CYP2D22 in CVP mice were significantly higher by ~40% than those in GFP mice (0.98 ± 0.03 vs. 0.58 ± 0.02, $p < 0.05$) (Fig. 5).

We also quantified various transporters due to their importance in drug disposition, including ABCB11 (Bsep), ABCB1A/B (P-gp), ABCC3 (Mrp3), ABCG2 (Bcrp), SLC22A2 (Oct2), SLC22A7 (Oat2), SLCO1A1 (Oatp1a1), and SLCO1A4 (Oatp1a4). Similar to CYP3A16 and CYP2D22, there were no significant differences in the protein levels of ABCB11 between CVNP and CVP or between GFNP and GFP; however, the protein levels of ABCB11 in CVP mice were significantly greater (~37%) than those in GFP mice (1.3 ± 0.07 vs. 0.82 ± 0.03, $p < 0.05$) (Fig. 6). We also observed significantly decreased protein abundance of SLCO1A1 in GFP mice compared to CVP mice (1.20 ± 0.03 vs. 2.20 ± 0.03, $p < 0.001$). The protein levels of

DMD Fast Forward. Published on June 4, 2020 as DOI: 10.1124/dmd.120.000039
This article has not been copyedited and formatted. The final version may differ from this version.

SLCO1A4 in GFP mice were significantly higher than those in CVP mice (0.71 ± 0.03 vs. 0.42 ± 0.03, $p < 0.05$), but there were no significant differences between GFNP and CVNP mice (Fig. 6). Pregnancy significantly increased the protein levels of SLC22A7 ~60% in GF mice (0.87 ± 0.04 vs. 0.55 ± 0.02, $p < 0.05$), but not in CV mice. No significant changes were observed in the abundance of ABCB1A/B, ABCC3 and ABCG2 proteins due to pregnancy or the microbiome.

Activity of hepatic Cyp3a enzymes determined by liver microsomal incubations

To confirm pregnancy-induced changes in protein expression of Cyp3a enzymes, microsomal incubations were performed to determine Cyp3a activity. We used a luciferin CYP3A probe to measure the amount of metabolite formed at a single incubation time point, which all fell within the linear range of product formation. Liver microsomes from CVP mice exhibited ~30-fold higher CYP3A activities ($p < 0.05$) than those from CVNP mice, whereas liver microsomes from GFP mice showed only a ~3-fold induction ($p < 0.05$) of CYP3A activity compared to GFNP mice (Fig. 7). Furthermore, the addition of ketoconazole (a potent, known CYP3A inhibitor) at 5 μM completely abolished metabolite formation with microsomes from both CV and GF mice (Fig. 7), suggesting that the enzymatic activity was due to CYP3A enzymes. Blank control and human recombinant CYP3A4 controls were also assayed in parallel to verify assay functionality (data not shown).

Quantification of plasma bile acids and steroid hormones

Because secondary bile acids generated by the gut microbiome may play an important role in regulating the expression of certain DMETs including Cyp3a enzymes (Nelson *et al.*, 2004; Chu *et al.*, 2013), we quantified plasma concentrations of primary and secondary bile acids in all mice by LC-MS/MS.

DMD Fast Forward. Published on June 4, 2020 as DOI: 10.1124/dmd.120.000039
This article has not been copyedited and formatted. The final version may differ from this version.

The plasma concentrations of the primary bile acids, αMCA and βMCA, in GFNP and GFP mice were lower than those in CVNP and CVP mice (Fig. 8). Pregnancy significantly increased the plasma concentrations of β-MCA in CV mice, but had no effect in GF mice. The microbiome had the opposite effect on taurine conjugates, with higher plasma concentrations of T-αMCA and T-βMCA in GF mice than in CV mice, regardless of pregnancy. The plasma concentrations of CA were increased ~14-fold by pregnancy in CV mice with no significant changes between GFP and GFNP mice. Moreover, the plasma concentrations of CA in GF mice were significantly lower than those in CV mice regardless of pregnancy (Fig. 8). The pattern of plasma concentrations of UDCA in all mice was similar to CA. Neither pregnancy nor the microbiome significantly affected the plasma concentrations of taurine conjugates of CA, CDCA and UDCA, with the exception that the plasma concentrations of T-CA in GFNP mice were 55 times greater than those in CVNP mice (Fig. 8).

As expected, the plasma concentrations of most of secondary bile acids were lower in GF mice versus CV mice, likely due to the lack of gut bacteria to synthesize them from primary bile acids (Fig. 9 and Supplemental Table S3). The plasma concentrations of DCA, HDCA, LCA, ωMCA, T-ωMCA, T-DCA, and T-LCA in GF mice were all significantly decreased versus those in CV mice, regardless of pregnancy (Fig. 9). Interestingly, in addition to a decrease in plasma concentrations of LCA in GFNP mice compared to CVNP mice (~11-fold decrease, $p < 0.05$), there was a further decrease of ~5-fold by pregnancy from GFNP to GFP mice ($p < 0.05$). Pregnancy also seemed to affect the production of some secondary bile acids. For example, pregnancy increased the plasma concentration of DCA ~7-fold ($p < 0.05$) in CV mice, but had no effect in GF mice. Pregnancy also significantly increased the plasma concentrations of HDCA in CV mice (9-fold, $p < 0.05$), but caused a 4-fold reduction ($p < 0.05$) in GF mice. Neither

pregnancy nor the microbiome significantly affected the plasma concentrations of THDCA (Fig. 9). With respect to MDCA, pregnancy significantly increased its plasma concentrations only in CV mice, but not in GF mice (Fig. 9). As expected, the plasma concentrations of MDCA were decreased in GF mice versus CV mice regardless of pregnancy, but the changes seemed to be small (Fig. 9 and Supplemental Table S3).

Pregnancy-related steroid hormones have been shown to regulate the expression of DMETs. Therefore, we also determined plasma concentrations of steroid hormones in all mice. As expected, pregnancy significantly increased the plasma concentrations of various steroid hormones, including 11-deoxycorticosterone, 17-OH-pregnenolone, 17-OH-progesterone, corticosterone, cortisol and progesterone, 38-fold to 125-fold in both CV and GF mice (Fig. 10 and Supplemental Table S4). The lack of the microbiome did not seem to alter pregnancy-induced levels of these hormones. The plasma concentrations of aldosterone and cortisone were significantly elevated by pregnancy in GF mice, but not in CV mice (Fig. 10). The plasma concentrations of estradiol were slightly but significantly decreased by pregnancy in CV mice, but not in GF mice. The lack of the microbiome did not affect the plasma concentrations of estradiol in both pregnant and non-pregnant mice (Fig. 10). On the other hand, we did not observe significant effects of pregnancy or the microbiome on pregnenolone, estrone and DHEA.

Discussion

In this study, we investigated the combined effects of pregnancy and microbiome on hepatic DMETs. This study used the same C57BL/6 strain as previous studies that investigated the effects of microbiome on hepatic DMETs in male mice (Selwyn *et al.*, 2015, 2016). Both this

and the previous studies showed a downward trend in mRNA of *Cyp3a* isoforms in GF versus CV mice; however, the magnitude of down-regulation observed in this study was much less pronounced. This could be due to sex-difference. The previous studies also reported a significant induction of *Cyp4a* genes by the microbiome knockout, whereas we did not. Again, this could be due to *Cyp4a* genes which are sex-divergent (Renaud *et al.*, 2011). Regulation of *Cyp4a14* was strongly influenced by androgen (Zhang and Klaassen, 2013), which is expectedly low in our female mice. Other factors that are known to control the gut microbiome ecosystems (e.g., age of mice, diet, and housing conditions) and might be different between this and previous studies could also potentially contribute to the discrepancy.

We previously showed that pregnancy alters hepatic DMETs in conventional FVB mice (Shuster *et al.*, 2013). Overall, our results are in good agreement with our previous studies. For example, we reported that *Cyp3a11* mRNA was decreased, whereas mRNA of *Cyp3a16* and *Cyp3a41* was increased during pregnancy. Consistently, this study also showed down-regulation and induction of *Cyp3a11* and *Cyp3a16/Cyp3a41*, respectively, by pregnancy in CV mice. We previously reported significant down-regulation of *Cyp2c* genes and *Mrp3*/*Abcc3* by pregnancy similar to this study in CV mice (Shuster *et al.*, 2013). There are some inconsistencies in the magnitude of pregnancy-induced change for some DMETs between this and our previous studies. For example, this study showed a 20.6-fold induction of *Cyp3a16* by pregnancy, while our previous studies reported an induction of only 60% on the same gd 15 (Shuster *et al.*, 2013). Our previous studies used FVB mice. The two different mouse strains are known to possess significantly different basal microbiota (Ahn *et al.*, 2018). Thus, the difference in mouse strain may contribute to the different magnitude of pregnancy-induced change for some DMETs between this and our previous studies.

DMD Fast Forward. Published on June 4, 2020 as DOI: 10.1124/dmd.120.000039
This article has not been copyedited and formatted. The final version may differ from this version.

The *Cyp3a* isoforms (*Cyp3a11*, *Cyp3a16, Cyp3a41* and *Cyp3a44*) were of particular interest because of the prominent role of their human CYP3A4 homolog in drug metabolism. We therefore systematically examined their mRNA and protein expression along with catalytic activity. We found that *Cyp3a11* mRNA was significantly decreased by pregnancy in both CV and GF mice, but with a much greater magnitude of down-regulation in GF versus CV mice. Down-regulation of *Cyp3a11* mRNA by pregnancy has been reported in our previous studies in CV mice, but the mechanistic reasoning is unknown (Zhang *et al.*, 2008; Shuster *et al.*, 2013). The greater magnitude of down-regulation of *Cyp3a11* mRNA by pregnancy in GF mice could be due to the combined effects of the lack of secondary bile acids, which would otherwise compensate for the decreased *Cyp3a11* gene expression during pregnancy in CV mice. Yet, targeted proteomics revealed an opposite effect of pregnancy on the protein levels of CYP3A11, with a comparable 2-fold induction in both CV and GF mice. In contrast to *Cyp3a11,* the mRNA levels of all other *Cyp3a* isoforms were induced by pregnancy in both CV and GF mice. Although the mRNA levels of these *Cyp3a* isoforms in CVP and GFP mice were comparable, the fold-induction in GF mice was generally much greater than that in CV mice (e.g., 128-fold in GF mice versus 20.6-fold in CV mice for *Cyp3a16*) (Table 1). This was due to the lower baseline levels of these *Cyp3a* genes in GFNP mice compared with CVNP mice which were likely caused by the lack of secondary bile acids. Surprisingly, pregnancy induced the protein levels of CYP3A16 and CYP3A41 in CV mice, but had limited effect in GF mice. Although circadian patterns of *Cyp* mRNA transcripts have been reported (Zhang *et al.*, 2009), all mice were sacrificed around the same time of day, and thus the contribution of time of tissue collection is unlikely to be the source of changes observed. Next, we examined the effects of pregnancy and microbiome on the overall CYP3A activity. At present, it is not possible to determine activities

of individual CYP3A isoforms due to the lack of specific probes or selective inhibitors for individual mouse CYP3A isoforms. Thus, the CYP3A activities we measured reflected the overall, combined activities of all CYP3A isoforms. The CYP3A activities were significantly induced by pregnancy in both CV and GF mice, but with a much greater induction in CV mice versus GF mice. The activity data agreed with the overall trend of pregnancy-induced increase in CYP3A protein and are also consistent with our previous studies showing that the mouse CYP3A activities for testosterone and glyburide were significantly induced by pregnancy (Zhang *et al.*, 2008; Shuster *et al.*, 2014). However, for the first time, we showed that the microbiome can significantly alter the magnitude of pregnancy-induction of CYP3A activity. The lower pregnancy-induction of CYP3A activity in GF mice could reflect only the activities of the CYP3A isoforms other than CYP3A11 that were not induced at the protein level (Fig. 5). Future studies are needed to explore the mechanisms of microbiome-induced changes in CYP3A activity.

There was a disconnection between the mRNA and protein expression data for many DMETs in addition to *Cyp3a11* as described above. For example, pregnancy drastically decreased the mRNA levels of *Cyp2c50* and *Cyp2c54*, but had no significant impact on their protein levels in both CV and GF mice. Likewise, the mRNA levels of *Abcc3* were significantly decreased by pregnancy in CV and GF mice, but its protein levels were not affected by pregnancy at all. These inconsistencies could be due to the relatively small sample size and large variations in analysis (e.g., proteomics) for certain DMETs, yet the data for CYP3A isoforms seem to be reliable because both the mRNA and/or activity data for the CYP3A isoforms are fully consistent with previous studies. The discrepancy between mRNA and protein expression is not uncommon, and could be due to post-transcriptional or epigenomic regulation of gene

expression as shown in numerous studies (Martínez-Jiménez *et al.*, 2007; Takagi *et al.*, 2008; Smutny *et al.*, 2013; Wang *et al.*, 2019). Recent studies showed that the gut bacteria *Akkermansia muciniphila* can affect the concentration of N6-methyladenosine (m6A) in the intestines and the liver, and m6A methylation can greatly alter RNA transcription processes, leading to epitranscriptomic changes that may explain the gap between mRNA and protein data (Zhao *et al.*, 2017; Miro-Blanch and Yanes, 2019). MicroRNA (miRNA) modifiers can also alter the transcript-protein relationship. A recent study reported bacteria phylum such as *Firmicutes, Bacteroidetes* and *Proteobacteria* have significant effects on miRNA expression in humans (Yuan *et al.*, 2018). Changes in miRNA expression due to bacteria shift or the microbiome knockout could also lead to changes in downstream gene regulation and result in variations in gene translation. Future studies are needed to explore the mechanisms of microbiome-induced disconnection between mRNA and protein expression of DMETs.

Cortisol has been shown to induce the expression of CYP3A through activation of GR which in turn induces PXR and then PXR induces transcription of CYP3A expression (Sachar *et al.*, 2019). This could be the potential mechanism by which hepatic CYP3A is induced during pregnancy. Supporting this hypothesis, the plasma concentrations of cortisol were markedly increased by pregnancy in both CV and GF mice and the mRNA levels of all *Cyp3a* isoforms but *Cyp3a11* were induced by pregnancy. Secondary bile acids have been shown to be PXR ligands that can induce CYP3A (Dempsey *et al.*, 2019). This explains our findings that the baseline mRNA levels of all *Cyp3a* isoforms in GFNP mice were generally lower than those in CVNP mice. However, the absence of secondary bile acids did not affect the induction of *Cyp3a16* and *Cyp3a41* mRNA by pregnancy, which is consistent with the finding that pregnancy-induced hormone production was generally not affected by the microbiome knockout. This suggests that

the lack of microbiome does not interfere with pregnancy-mediated induction of *Cyp3a* gene transcription, which is mediated by increased production of steroid hormones during pregnancy. However, the microbiome can alter the magnitude of induction by changing the baseline expression of *Cyp3a* genes (Fig. 2) or influencing pregnancy-induced Cyp3a protein expression (Fig. 5) and hence activity (Fig. 7).

In summary, we have shown, for the first time, that the microbiome can affect hepatic DMETs in pregnant mice by altering the magnitude of pregnancy-induced fold-change in the expression (mRNA or protein) and/or the activity of hepatic DMETs. Caution should be taken to translate the data to drug disposition *in vivo* due to disconnection between mRNA and protein, relatively small sample size, and large variation in analysis of certain DMETs. Nevertheless, these results provide the basis for further mechanistic investigation of microbiome-mediated changes in hepatic DMETs and drug disposition during pregnancy. Future studies should also examine the impact of microbiome on DMETs in other organs of pregnant mice important for drug disposition including the small intestine.

DMD Fast Forward. Published on June 4, 2020 as DOI: 10.1124/dmd.120.000039
This article has not been copyedited and formatted. The final version may differ from this version.

Acknowledgements

We would like to thank Dr. Adeline Hajjar for her assistance and guidance in the maintenance and breeding of germ-free mice.

Author Contributions

Participated in research design: Han, Wang, Shi, Bammler, Cui, and Mao

Conducted experiments: Han and Pershutkina

Contributed in new reagents or analytic tools: Han, Wang, Shi, Dempsey, and Dutta

Performed data analysis: Han, Wang, Shi, Dempsey, and Dutta

Wrote or contributed to the writing of the manuscript: Han, Wang, Shi, Dempsey, Dutta, Bammler, Cui, and Mao

References

Ahn I-S, Lang J, Olsen C, Ying Z, Zhang G, Byun HR, Zhao Y, Kurt Z, Lusis AJ, Hsaio E, Gomez-Pinilla F, and Yang X (2018) Host Genetic Background and Gut Microbiota Contribute to Differential Metabolic Responses to High Fructose Consumption in Mice. *bioRxiv* 439786.

Alnouti Y, Csanaky IL, and Klaassen CD (2008) Quantitative-profiling of bile acids and their conjugates in mouse liver, bile, plasma, and urine using LC-MS/MS. *J Chromatogr B Anal Technol Biomed Life Sci* **873**:209–217.

Basit A, Amory JK, and Prasad B (2018) Effect of Dose and 5α-Reductase Inhibition on the Circulating Testosterone Metabolite Profile of Men Administered Oral Testosterone. *Clin Transl Sci* **11**:513–522.

Beigi RH, Noguchi L, Brown G, Piper J, and Watts DH (2016) Performing drug safety research during pregnancy and lactation: Biomedical HIV prevention research as a template. *J Women's Heal* **25**:761–766.

Benjamini Y, and Hochberg Y (1995) Controlling the False Discovery Rate: A Practical and Powerful Approach to Multiple Testing. *J R Stat Soc B* **57**:289–300.

Bhatt DK, and Prasad B (2018) Critical Issues and Optimized Practices in Quantification of Protein Abundance Level to Determine Interindividual Variability in DMET Proteins by LC-MS/MS Proteomics. *Clin Pharmacol Ther* **103**:619-630.

Chen Y, Lun ATL, and Smyth GK (2016) From reads to genes to pathways: Differential expression analysis of RNA-Seq experiments using Rsubread and the edgeR quasi-

likelihood pipeline. Version 2. *F1000Res* **5**:1438.

Chu X, Bleasby K, and Evers R (2013) Species differences in drug transporters and implications for translating preclinical findings to humans. *Expert Opin Drug Metab Toxicol* **9**:237-252.

Claus SP, Ellero SL, Berger B, Krause L, Bruttin A, Molina J, Paris A, Want EJ, de Waziers I, Cloarec O, Richards SE, Wang Y, Dumas M-E, Ross A, Rezzi S, Kochhar S, Van Bladeren P, Lindon JC, Holmes E, and Nicholson JK (2011) Colonization-induced host-gut microbial metabolic interaction. *MBio* **2**:e00271-10.

Dempsey JL, Wang D, Siginir G, Fei Q, Raftery D, Gu H, and Yue Cui J (2019) Pharmacological Activation of PXR and CAR Downregulates Distinct Bile Acid-Metabolizing Intestinal Bacteria and Alters Bile Acid Homeostasis. *Toxicol Sci* **168**:40–60.

Dussault I, Yoo HD, Lin M, Wang E, Fan M, Batta AK, Salen G, Erickson SK, and Forman BM (2003) Identification of an endogenous ligand that activates pregnane X receptor-mediated sterol clearance. *Proc Natl Acad Sci U S A* **100**:833–838.

FDA (2018) Drug Safety Priorities 2018.

Feghali M, Venkataramanan R, and Caritis S (2015) Pharmacokinetics of drugs in pregnancy. *Semin Perinatol* **39**:512–519.

Helldén A, and Madadi P (2013) Pregnancy and pharmacogenomics in the context of drug metabolism and response. *Pharmacogenomics* **14**:1779-1791.

Isoherranen N, and Thummel KE (2013) Drug metabolism and transport during pregnancy: how does drug disposition change during pregnancy and what are the mechanisms that cause such changes? *Drug Metab Dispos* **41**:256–62.

Klaassen CD, and Cui JY (2015) Review: Mechanisms of How the Intestinal Microbiota Alters the Effects of Drugs and Bile Acids. *Drug Metab Dispos* **43**:1505–21.

Kliewer SA, Moore JT, Wade L, Staudinger JL, Watson MA, Jones SA, McKee DD, Oliver BB, Willson TM, Zetterström RH, Perlmann T, and Lehmann JM (1998) An orphan nuclear receptor activated by pregnanes defines a novel steroid signaling pathway. *Cell* **92**:73–82.

Kong B, Wang L, Chiang JYL, Zhang Y, Klaassen CD, and Guo GL (2012) Mechanism of tissue-specific farnesoid X receptor in suppressing the expression of genes in bile-acid synthesis in mice. *Hepatology* **56**:1034–1043.

Lee C, Ding X, and Riddick DS (2013) Downregulation of mouse hepatic CYP3A protein by 3-methylcholanthrene does not require cytochrome P450-dependent metabolism. *Drug Metab Dispos* **41**:1782–6.

Li CY, Lee S, Cade S, Kuo L-J, Schultz IR, Bhatt DK, Prasad B, Bammler TK, and Cui JY (2017) Novel Interactions between Gut Microbiome and Host Drug-Processing Genes Modify the Hepatic Metabolism of the Environmental Chemicals Polybrominated Diphenyl Ethers. *Drug Metab Dispos* **45**:1197–1214.

Liao MZ, Gao C, Phillips BR, Neradugomma NK, Han LW, Bhatt DK, Prasad B, Shen DD, and Mao Q (2018) Quantitative Proteomics Reveals Changes in Transporter Protein Abundance in Liver, Kidney and Brain of Mice by Pregnancy. *Drug Metab Lett* **12**:145–152.

Martínez-Jiménez CP, Jover R, Donato MT, Castell J V, and Gómez-Lechón MJ (2007) Transcriptional regulation and expression of CYP3A4 in hepatocytes. *Curr Drug Metab* **8**:185–94.

Miro-Blanch J, and Yanes O (2019) Epigenetic regulation at the interplay between gut microbiota and host metabolism. *Front Genet* **10**:638.

Nelson DR, Zeldin DC, Hoffman SMG, Maltais LJ, Wain HM, and Nebert DW (2004) Comparison of cytochrome P450 (CYP) genes from the mouse and human genomes, including nomenclature recommendations for genes, pseudogenes and alternative-splice variants. *Pharmacogenetics* **14**:1-18.

Nuriel-Ohayon M, Neuman H, and Koren O (2016) Microbial changes during pregnancy, birth, and infancy. *Front Microbiol* **7**:1031.

Paine MF, Khalighi M, Fisher JM, Shen DD, Kunze KL, Marsh CL, Perkins JD, and Thummel KE (1997) Characterization of interintestinal and intraintestinal variations in human CYP3A-dependent metabolism. *J Pharmacol Exp Ther* **283**:1552–1562.

Papacleovoulou G, Abu-Hayyeh S, and Williamson C (2011) Nuclear receptor-driven alterations in bile acid and lipid metabolic pathways during gestation. *Biochim Biophys Acta.* **1812**:879-87.

Pariente G, Leibson T, Carls A, Adams-Webber T, Ito S, and Koren G (2016) Pregnancy-Associated Changes in Pharmacokinetics: A Systematic Review. *PLoS Med* **13**:e1002160.

Patro R, Duggal G, Love M, Irizarry R, and Kingsford C (2015) Salmon provides accurate, fast, and bias-aware transcript expression estimates using dual-phase inference. *bioRxiv* 021592.

Perloff MD, von Moltke LL, Cotreau MM, and Greenblatt DJ (1999) Unchanged cytochrome P450 3A (CYP3A) expression and metabolism of midazolam, triazolam, and dexamethasone in mdr(-/-) mouse liver microsomes. *Biochem Pharmacol* **57**:1227-1232

Prasad B, Bhatt DK, Johnson K, Chapa R, Chu X, Salphati L, Xiao G, Lee C, Hop CECA, Mathias A, Lai Y, Liao M, Humphreys WG, Kumer SC, and Unadkat JD (2018) Abundance of phase 1 and 2 drug-metabolizing enzymes in alcoholic and hepatitis C cirrhotic livers: A quantitative targeted proteomics study. *Drug Metab Dispos* **46**:943–952.

Renaud HJ, Cui JY, Khan M, and Klaassen CD (2011) Tissue distribution and gender-divergent expression of 78 cytochrome p450 mRNAs in mice. *Toxicol Sci* **124**:261–277.

Ridlon JM, Kang DJ, and Hylemon PB (2006) Bile salt biotransformations by human intestinal bacteria. *J Lipid Res* **47**:241-259.

Robinson MD, McCarthy DJ, and Smyth GK (2009) edgeR: A Bioconductor package for differential expression analysis of digital gene expression data. *Bioinformatics* **26**:139–140.

Sachar M, Kelly EJ, and Unadkat JD (2019) Mechanisms of CYP3A Induction During Pregnancy: Studies in HepaRG Cells. *AAPS J* **21**:45.

Selwyn FP, Cheng SL, Bammler TK, Prasad B, Vrana M, Klaassen C, and Cui JY (2015) Developmental Regulation of Drug-Processing Genes in Livers of Germ-Free Mice. *Toxicol Sci* **147**:84–103.

Selwyn FP, Cheng SL, Klaassen CD, and Cui JY (2016) Regulation of hepatic drug-metabolizing enzymes in germ-free mice by conventionalization and probiotics. *Drug Metab Dispos* **44**:262–274.

Sharma A, Buschmann MM, and Gilbert JA (2019) Pharmacomicrobiomics: The Holy Grail to Variability in Drug Response? *Clin Pharmacol Ther* **106**:317-328.

Shuster DL, Bammler TK, Beyer RP, Macdonald JW, Tsai JM, Farin FM, Hebert MF, Thummel

KE, and Mao Q (2013) Gestational age-dependent changes in gene expression of metabolic enzymes and transporters in pregnant mice. *Drug Metab Dispos* **41**:332–42.

Shuster DL, Risler LJ, Liang CKJ, Rice KM, Shen DD, Hebert MF, Thummel KE, and Mao Q (2014) Maternal-fetal disposition of glyburide in pregnant mice is dependent on gestational age. *J Pharmacol Exp Ther* **350**:425–434.

Smutny T, Mani S, and Pavek P (2013) Post-translational and post-transcriptional modifications of pregnane X receptor (PXR) in regulation of the cytochrome P450 superfamily. *Curr Drug Metab* **14**:1059–69.

Soneson C, Love MI, and Robinson MD (2015) Differential analyses for RNA-seq: transcript-level estimates improve gene-level inferences. *F1000Research* **4**:1521.

Spanogiannopoulos P, Bess EN, Carmody RN, and Turnbaugh PJ (2016) The microbial pharmacists within us: a metagenomic view of xenobiotic metabolism. *Nat Rev Microbiol* **14**:273–287.

Staudinger JL, Goodwin B, Jones SA, Hawkins-Brown D, MacKenzie KI, LaTour A, Liu Y, Klaassen CD, Brown KK, Reinhard J, Willson TM, Koller BH, and Kliewer SA (2001) The nuclear receptor PXR is a lithocholic acid sensor that protects against liver toxicity. *Proc Natl Acad Sci U S A* **98**:3369–3374.

Takagi S, Nakajima M, Mohri T, and Yokoi T (2008) Post-transcriptional regulation of human pregnane X receptor by micro-RNA affects the expression of cytochrome P450 3A4. *J Biol Chem* **283**:9674–80.

Tasnif Y, Morado J, and Hebert M (2016) Pregnancy-related pharmacokinetic changes. *Clin*

Pharmacol Ther **100**:53–62.

Wahlström A, Kovatcheva-Datchary P, Ståhlman M, Bäckhed F, and Marschall H-U (2017) Crosstalk between Bile Acids and Gut Microbiota and Its Impact on Farnesoid X Receptor Signalling. *Dig Dis* **35**:246–250.

Wang H, Chen J, Hollister K, Sowers LC, and Forman BM (1999) Endogenous bile acids are ligands for the nuclear receptor FXR/BAR. *Mol Cell* **3**:543–53.

Wang S, Chen L, Wang Q, He Z, Chen S, Zhang H, Li H, Guo P, Li Q, Zhang R, Xing X, Zeng X, Lin W, Xiao Y, Dong G, Ma L, Gurram N, Zhang A, Chen W, and Li D (2019) Strain differences between CD-1 and C57BL/6 mice in expression of metabolic enzymes and DNA methylation modifications of the primary hepatocytes. *Toxicology* **412**:19–28.

Yuan C, Burns MB, Subramanian S, and Blekhman R (2018) Interaction between Host MicroRNAs and the Gut Microbiota in Colorectal Cancer. *mSystems* **3**:e00205-17.

Zhang H, Wu X, Wang H, Mikheev AM, Mao Q, and Unadkat JD (2008) Effect of pregnancy on cytochrome P450 3a and P-glycoprotein expression and activity in the mouse: mechanisms, tissue specificity, and time course. *Mol Pharmacol* **74**:714–23.

Zhang Y, and Klaassen CD (2013) Hormonal regulation of Cyp4a isoforms in mouse liver and kidney. *Xenobiotica* **43**:1055–1063.

Zhang YKJ, Yeager RL, and Klaassen CD (2009) Circadian expression profiles of drug-processing genes and transcription factors in mouse liver. *Drug Metab Dispos* **37**:106–115.

Zhao BS, Roundtree IA, and He C (2017) Post-transcriptional gene regulation by mRNA modifications. *Nat Rev Mol Cell Biol* **18**:31-42.

Funding

This work was supported by The Drug Metabolism, Transport and Pharmacogenomic Research Program (DMTPR) at the University of Washington, and in part by the National Center for Advancing Translational Science of the National Institutes of Health [Grant TL1TR000422], the National Institute of Environmental Health Sciences [Grant P30ES007033], the National Institute on Drug Abuse [Grant P01DA032507], and the National Institute of General Medical Sciences [Grant R01GM111381].

DMD Fast Forward. Published on June 4, 2020 as DOI: 10.1124/dmd.120.000039
This article has not been copyedited and formatted. The final version may differ from this version.

Figure Legends

Figure 1. Comparison of expression of selected genes determined by RNA-seq and qRT-PCR analysis. Log2 fold-change is relative to the CVNP group for both RNA-seq and qRT-PCR data. Shown are means ± SD of gene expression data from 5 – 6 different mouse liver tissues.

Figure 2. Effect of pregnancy and microbiome on mRNA expression of hepatic Phase I enzymes. Shown are boxplots with individual scatters of RNA-seq analysis data of hepatic phase I enzymes from female C57BL/6 mice. Data illustrates individual log2 counts-per-million for each DMET. All pregnant mice used were on gestation day 15. *$FDR < 0.1$; **$FDR < 0.01$; ***$FDR < 0.001$. CVNP, conventional non-pregnant mice; CVP, conventional pregnant mice; GFNP, germ-free non-pregnant mice; GFP, germ-free pregnant mice.

Figure 3. Effect of pregnancy and microbiome on mRNA expression of hepatic Phase II enzymes. Shown are boxplots with individual scatters of RNA-seq analysis data of hepatic phase II enzymes from female C57BL/6 mice. Data illustrates individual log2 counts-per-million for each DMET. All pregnant mice used were on gestation day 15. *$FDR < 0.1$; **$FDR < 0.01$; ***$FDR < 0.001$. CVNP, conventional non-pregnant mice; CVP, conventional pregnant mice; GFNP, germ-free non-pregnant mice; GFP, germ-free pregnant mice.

Figure 4. Effect of pregnancy and microbiome on mRNA expression of hepatic transporters. Shown are boxplots with individual scatters of RNA-seq analysis data of hepatic transporters from female C57BL/6 mice. Data illustrates individual log2 counts-per-million for

each DMET. All pregnant mice used were on gestation day 15. *$FDR < 0.1$; **$FDR < 0.01$; ***$FDR < 0.001$. CVNP, conventional non-pregnant mice; CVP, conventional pregnant mice; GFNP, germ-free non-pregnant mice; GFP, germ-free pregnant mice.

Figure 5. Effect of pregnancy and microbiome on protein expression of hepatic Cyp enzymes. Shown are boxplots with individual data points of relative protein levels of hepatic Cyp enzymes in C57BL/6 female mice. Shown are means ± SE for selected enzymes or transporters in the liver from 4-6 mice. Data illustrates ratio-of-ratio estimates for each DMET. All pregnant mice used were on gestation day 15. *$p < 0.05$; **$p < 0.01$; ***$p < 0.001$ by Wilcoxon signed-rank test. CVNP, conventional non-pregnant mice; CVP, conventional pregnant mice; GFNP, germ-free non-pregnant mice; GFP, germ-free pregnant mice.

Figure 6. Effect of pregnancy and microbiome on protein expression of hepatic transporters. Shown are boxplots with individual data points of relative protein levels of hepatic transporters in C57BL/6 female mice. Shown are means ± SE for selected enzymes or transporters in the liver from 4-6 mice. Data illustrates ratio-of-ratio estimates for each DMET. All pregnant mice used were on gestation day 15. *$p < 0.05$; **$p < 0.01$; ***$p < 0.001$ by Wilcoxon signed-rank test. CVNP, conventional non-pregnant mice; CVP, conventional pregnant mice; GFNP, germ-free non-pregnant mice; GFP, germ-free pregnant mice.

Figure 7. Effect of pregnancy and microbiome on hepatic Cyp3a activity. Shown are boxplots of individual data points of hepatic Cyp3a activity which is presented as relative light

DMD Fast Forward. Published on June 4, 2020 as DOI: 10.1124/dmd.120.000039
This article has not been copyedited and formatted. The final version may differ from this version.

unit. Circles represent incubations without an inhibitor, and triangles indicate incubations in the presence of the inhibitor ketoconazole at 5 μM. Data shown are means ± SE of hepatic Cyp3a activity in liver microsomes isolated from 4-6 mice from one representative experiment. The experiment was done in triplicate and repeated, and similar results were obtained. All pregnant mice used were on gestation day 15. *$p < 0.05$; **$p < 0.01$; ***$p < 0.001$ by Wilcoxon signed-rank test. CVNP, conventional non-pregnant mice; CVP, conventional pregnant mice; GFNP, germ-free non-pregnant mice; GFP, germ-free pregnant mice.

Figure 8. **Effect of pregnancy and microbiome on plasma concentrations of primary bile acids.** Shown are boxplots with individual data points of plasma concentrations of primary bile acids in C57BL/6 female mice. Concentrations were determined using targeted LC-MS/MS quantification and reported as ng/ml. Shown are means ± SE for selected bile acids or steroid hormones in the plasma from 5-6 mice. All pregnant mice used were on gestation day 15. *$p < 0.05$; **$p < 0.01$; ***$p < 0.001$ by Wilcoxon signed-rank test. CVNP, conventional non-pregnant mice; CVP, conventional pregnant mice; GFNP, germ-free non-pregnant mice; GFP, germ-free pregnant mice.

Figure 9. **Effect of pregnancy and microbiome on plasma concentrations of secondary bile acids.** Shown are boxplots with individual data points of plasma concentrations of secondary bile acids in C57BL/6 female mice. Concentrations were determined using targeted LC-MS/MS quantification and reported as ng/ml. Shown are means ± SE for selected bile acids or steroid hormones in the plasma from 5-6 mice. All pregnant mice used were on gestation day 15. *$p <$

DMD Fast Forward. Published on June 4, 2020 as DOI: 10.1124/dmd.120.000039
This article has not been copyedited and formatted. The final version may differ from this version.

0.05; **$p < 0.01$; ***$p < 0.001$ by Wilcoxon signed-rank test. CVNP, conventional non-pregnant mice; CVP, conventional pregnant mice; GFNP, germ-free non-pregnant mice; GFP, germ-free pregnant mice.

Figure 10. **Effect of pregnancy and microbiome on plasma concentrations of steroid hormones.** Shown are boxplots with individual data points of plasma concentrations of steroid hormones in C57BL/6 female mice. Concentrations were determined using targeted LC-MS/MS quantification and reported as ng/ml. Shown are means ± SE for selected bile acids or steroid hormones in the plasma from 5-6 mice. All pregnant mice used were on gestation day 15. *$p < 0.05$; **$p < 0.01$; ***$p < 0.001$ by Wilcoxon signed-rank test. CVNP, conventional non-pregnant mice; CVP, conventional pregnant mice; GFNP, germ-free non-pregnant mice; GFP, germ-free pregnant mice.

DMD Fast Forward. Published on June 4, 2020 as DOI: 10.1124/dmd.120.000039
This article has not been copyedited and formatted. The final version may differ from this version.

Tables

Table 1. **Pregnancy and the microbiome alter mRNA expression of key DMETs in female C57BL/6 livers.** This list of genes was generated using the following filtration criteria: fold-change > 1.5 or < 0.65 and *FDR* < 0.1, on at least one comparison group between CVP and CVNP, GFP and GFNP, GFNP and CVNP, or GFP and CVP. Statistically significant differences with *FDR* values of < 0.1 are highlighted in bold.

Gene Symbol	CVP vs. CVNP		GFP vs. GFNP		GFNP vs. CVNP		GFP vs. CVP	
	Fold Change	*FDR*	Fold Change	*FDR*	Fold Change	*FDR*	Fold Change	*FDR*
Cyp17a1	1.7	0.28	**2.9**	**0.01**	0.9	1	1.6	0.704
Cyp26a1	**3.2**	**0.076**	**4.2**	**0.02**	0.9	1	1.1	0.996
Cyp26b1	**<0.1**	**<0.001**	**0.1**	**<0.001**	1.9	0.982	5	0.289
Cyp2b13	**0.1**	**<0.001**	**0.3**	**<0.001**	1.2	1	**5.3**	**<0.001**
Cyp2c37	**0.3**	**0.002**	0.6	0.152	1	1	1.8	0.401
Cyp2c38	**0.4**	**0.007**	1	0.965	1.3	1	**3**	**0.013**
Cyp2c39	1	0.983	**2.4**	**0.022**	1.1	1	2.7	0.154
Cyp2c50	**0.2**	**<0.001**	**0.5**	**0.001**	1	1	**2**	**0.066**
Cyp2c54	**0.4**	**0.001**	0.8	0.561	1	1	**2.2**	**0.074**
Cyp2c55	0.5	0.216	**0.1**	**<0.001**	2.8	0.319	0.8	0.974
Cyp2c67	**0.4**	**0.012**	0.6	0.279	1.4	1	2.3	0.238
Cyp2c69	1	0.998	**2.6**	**0.02**	0.6	0.982	1.6	0.708
Cyp2d40	**3.9**	**<0.001**	**5.4**	**<0.001**	0.7	1	1	1
Cyp2d9	**0.3**	**0.025**	**0.2**	**0.002**	1.8	1	1.1	1
Cyp2g1	**2.8**	**0.047**	**3.6**	**0.01**	0.6	1	0.8	0.964
Cyp39a1	**0.4**	**0.031**	**0.3**	**0.017**	1	1	0.9	0.999
Cyp3a11	0.6	0.29	**0.3**	**0.005**	0.6	0.953	0.3	0.131
Cyp3a16	**20.6**	**0.001**	**128**	**<0.001**	0.2	0.578	1.4	0.953
Cyp3a41a	**4.8**	**0.047**	**10.8**	**0.002**	0.6	1	1.4	0.941
Cyp3a41b	**74.2**	**<0.001**	**181.7**	**<0.001**	0.5	1	1.3	0.989
Cyp3a44	**14.3**	**<0.001**	**30.5**	**<0.001**	0.8	1	1.7	0.816
Cyp3a63-ps	**5.1**	**0.047**	**8.5**	**0.007**	0.9	1	1.5	0.926
Cyp4a14	**0.4**	**0.021**	**0.3**	**0.002**	1.2	1	0.9	0.958
Cyp4a31	**4.6**	**<0.001**	**5.3**	**<0.001**	1.1	1	1.3	0.909
Cyp4f13	**0.6**	**0.042**	0.8	0.329	0.8	1	1.1	0.987
Cyp4f15	**0.5**	**0.033**	**0.5**	**0.052**	1	1	1.1	0.976
Ugt1a10	0.9	0.977	**9.6**	**0.004**	0.2	0.439	2.4	0.689
Ugt1a5	**2.6**	**0.062**	**3.3**	**0.016**	0.5	0.949	0.7	0.833
Ugt1a6b	**0.3**	**0.042**	**0.3**	**0.023**	1	1	0.9	0.999
Ugt2b38	0.2	0.139	**<0.1**	**0.013**	0.5	1	0.1	0.408

DMD Fast Forward. Published on June 4, 2020 as DOI: 10.1124/dmd.120.000039
This article has not been copyedited and formatted. The final version may differ from this version.

Sult2a7	**0.2**	**0.061**	**0.2**	**0.031**	0.9	1	0.7	0.964
Sult3a1	**3.6**	**0.056**	**12.9**	**<0.001**	0.3	0.359	1	1
Sult3a2	**53.9**	**<0.001**	**226.7**	**<0.001**	0.2	0.605	0.9	1
Sult4a1	**287.7**	**<0.001**	3.5	0.333	5.2	1	0.1	0.129
Gsta2	0.6	0.215	**0.4**	**0.033**	2	0.605	1.5	0.782
Gstk1	**0.5**	**0.005**	**0.5**	**0.018**	1.1	1	1.2	0.901
Gstm2	**1.8**	**0.041**	1.4	0.248	1.4	1	1.1	0.984
Gstm3	**3.1**	**0.044**	0.6	0.456	2.5	0.564	0.5	0.625
Gstp1	**3.4**	**0.002**	**2.2**	**0.039**	0.9	1	0.6	0.635
Gstp2	**5.9**	**0.016**	1.8	0.505	0.9	1	0.3	0.386
Gstt1	**0.4**	**0.005**	**0.4**	**0.017**	0.8	1	0.9	0.976
Gstt3	1.5	0.177	**2**	**0.005**	0.8	1	1.1	0.951
Abca17	**103.3**	**<0.001**	**1779**	**<0.001**	0.1	0.757	1.2	0.989
Abca5	**2**	**0.025**	**3.3**	**<0.001**	0.8	1	1.3	0.768
Abca7	0.9	0.851	**0.5**	**0.006**	1.1	1	0.6	0.298
Abcb6	**0.6**	**0.019**	0.7	0.129	1	1	1.2	0.83
Abcc3	**0.3**	**0.025**	**0.1**	**<0.001**	1	1	0.5	0.613
Abcg5	**0.4**	**0.003**	**0.4**	**0.009**	1.3	1	1.4	0.696
Abcg8	**0.5**	**0.008**	**0.6**	**0.061**	1.2	1	1.4	0.613
Slc10a1	**0.4**	**0.02**	**0.5**	**0.045**	0.8	1	1	1
Slc16a1	**2**	**0.018**	1.6	0.142	0.9	1	0.7	0.625
Slc16a6	**16.2**	**<0.001**	**14.4**	**<0.001**	1.1	1	1	1
Slc17a2	**0.3**	**0.057**	**0.2**	**0.009**	0.9	1	0.6	0.816
Slc22a15	**0.5**	**0.008**	**0.5**	**0.028**	1.1	1	1.2	0.869
Slc22a2	**260.5**	**<0.001**	**561.5**	**<0.001**	0.4	1	0.8	0.984
Slc22a7	1.3	0.713	**3.1**	**0.004**	0.5	0.437	1.1	0.975
Slc24a3	**9.5**	**<0.001**	**6.6**	**<0.001**	1.3	1	0.9	0.969
Slc25a19	0.8	0.291	**0.6**	**0.015**	1.1	1	0.9	0.857
Slc25a28	**0.6**	**0.007**	**0.7**	**0.024**	0.9	1	0.9	0.953
Slc25a30	1.7	0.128	**2.2**	**0.01**	0.5	0.315	0.7	0.639
Slc25a37	**0.5**	**0.012**	**0.6**	**0.027**	0.9	1	1	1
Slc25a51	**0.6**	**0.026**	**0.3**	**<0.001**	1.8	0.181	1.1	0.951
Slc26a10	**0.4**	**0.079**	**0.3**	**0.006**	1.3	1	0.9	0.988
Slc26a4	**0.1**	**0.009**	**0.2**	**0.016**	1.2	1	1.6	0.947
Slc27a1	0.7	0.21	**0.6**	**0.018**	1.3	1	1	1
Slc35b1	**1.8**	**0.006**	**2.5**	**<0.001**	1	1	1.3	0.617
Slc35c1	1.3	0.254	**1.6**	**0.029**	0.9	1	1.1	0.953
Slc35c2	**1.7**	**0.003**	**2**	**<0.001**	0.9	1	1	1
Slc36a1	**2.3**	**0.001**	**2.7**	**<0.001**	0.9	1	1	1
Slc37a1	**11.6**	**<0.001**	**6.2**	**<0.001**	1.5	1	0.8	0.946
Slc38a4	**0.3**	**<0.001**	**0.3**	**<0.001**	1.1	1	1.2	0.951
Slc39a11	**1.4**	**0.18**	**2**	**<0.001**	0.9	1	1.3	0.626
Slc39a14	**2.3**	**0.013**	**2.1**	**0.022**	1.5	0.978	1.4	0.775
Slc41a2	**30.2**	**<0.001**	**28.1**	**<0.001**	1.1	1	1	1
Slc41a3	**4.3**	**0.001**	**3.5**	**0.002**	1.9	0.781	1.5	0.753
Slc43a1	**2.6**	**0.037**	**3.1**	**0.01**	1.1	1	1.3	0.934
Slc45a3	**3**	**0.001**	**2.1**	**0.027**	1.2	1	0.9	0.948
Slc4a1	**8**	**0.002**	**24**	**<0.001**	0.9	1	2.6	0.415
Slc4a9	**0.1**	**0.025**	**0.1**	**0.001**	3.9	0.359	1.9	0.914
Slc6a9	**6.1**	**<0.001**	**9**	**<0.001**	0.7	1	1.1	1

DMD Fast Forward. Published on June 4, 2020 as DOI: 10.1124/dmd.120.000039
This article has not been copyedited and formatted. The final version may differ from this version.

Slc7a15	**5**	**0.102**	**19.1**	**0.01**	0.1	0.554	0.4	0.786
Slc7a2	**0.4**	**0.013**	**0.5**	**0.058**	1.3	1	1.6	0.625
Slc7a7	**5**	**<0.001**	**2.9**	**0.003**	1.1	1	0.6	0.601
Slc8b1	**0.5**	**0.023**	**0.6**	**0.055**	0.8	1	0.9	0.958
Slc9a3	0.4	0.766	**74.3**	**0.005**	0.1	1	23.5	0.238
Slco1a4	**0.4**	**0.045**	**0.4**	**0.063**	1.1	1	1.2	0.945
Slco4c1	4.8	0.519	**17.8**	**0.035**	2.6	1	9.6	0.376

Figure 1

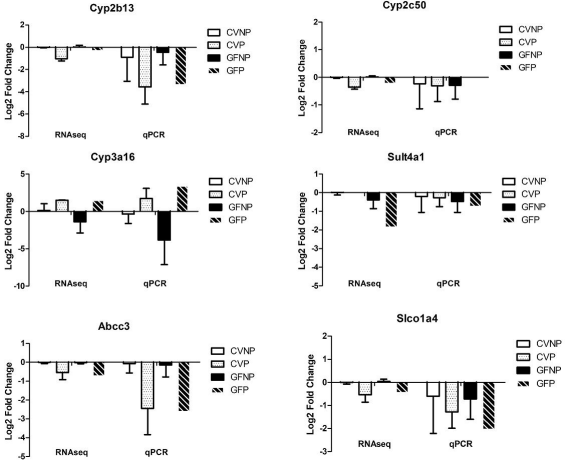
Cyp2b13
Log2 Fold Change
RNAseq
qPCR
CVNP
CVP
GFNP
GFP
Cyp2c50
Cyp3a16
Sult4a1
Abcc3
Slco1a4

Figure 2

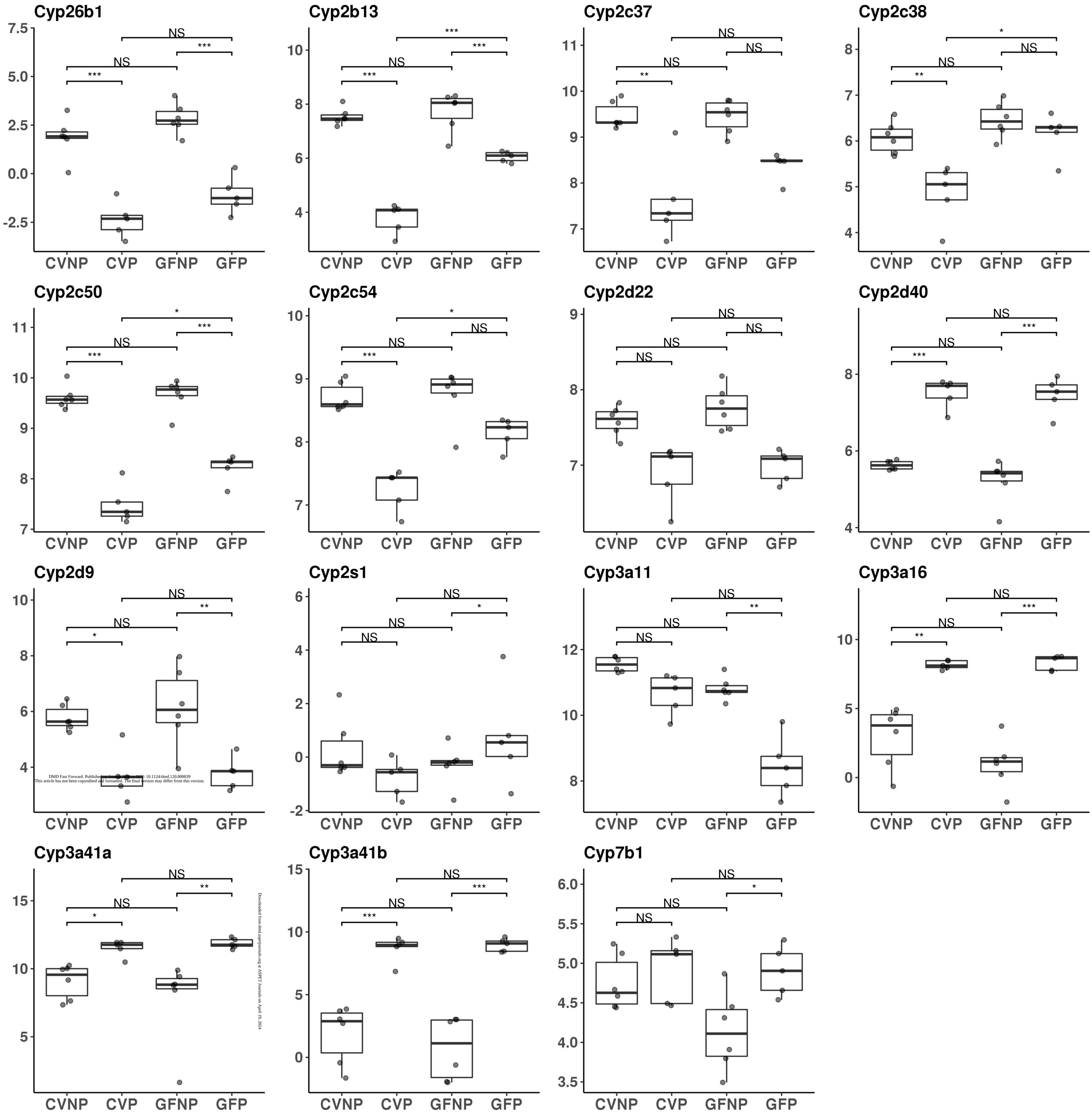

Figure 3

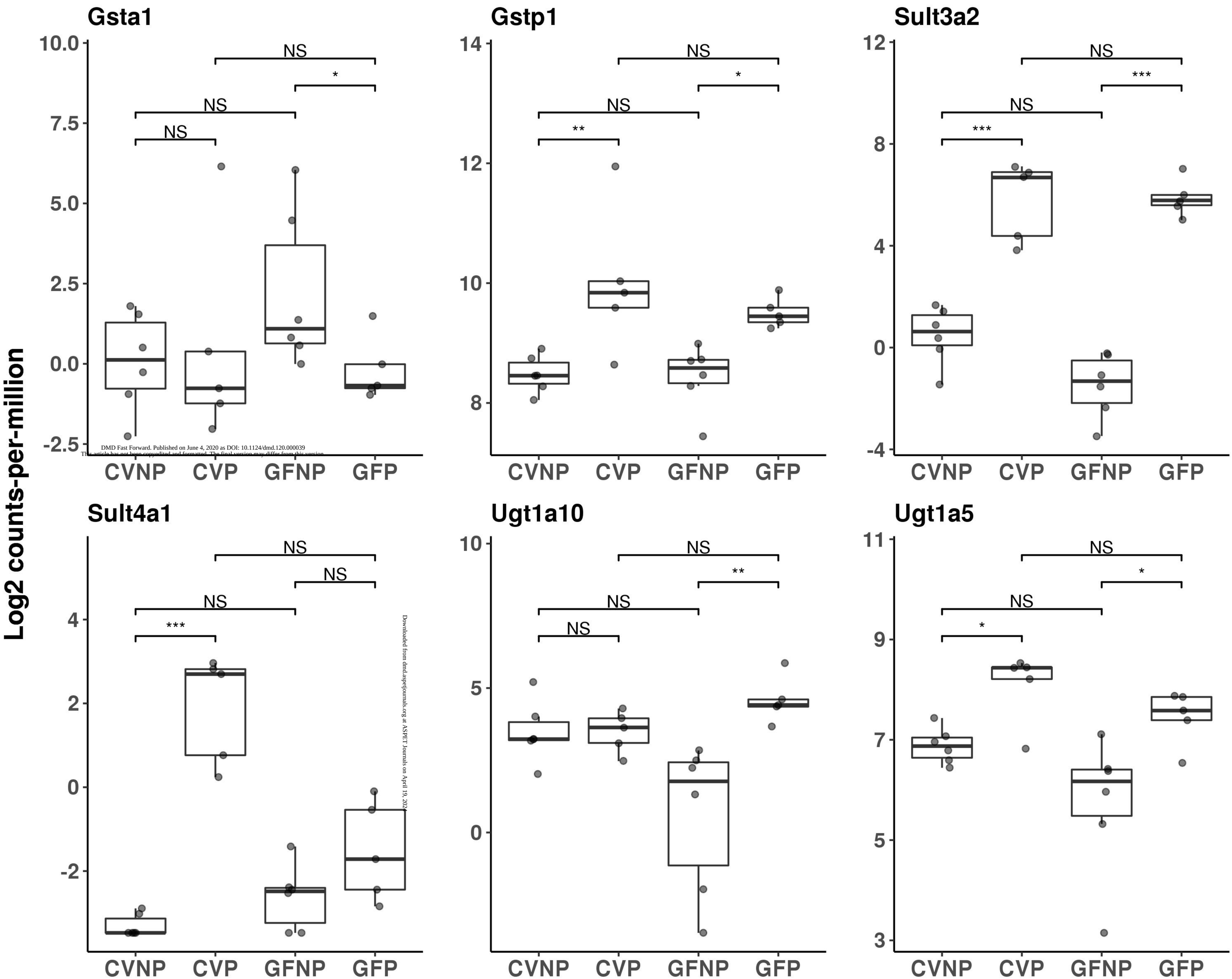

Figure 4

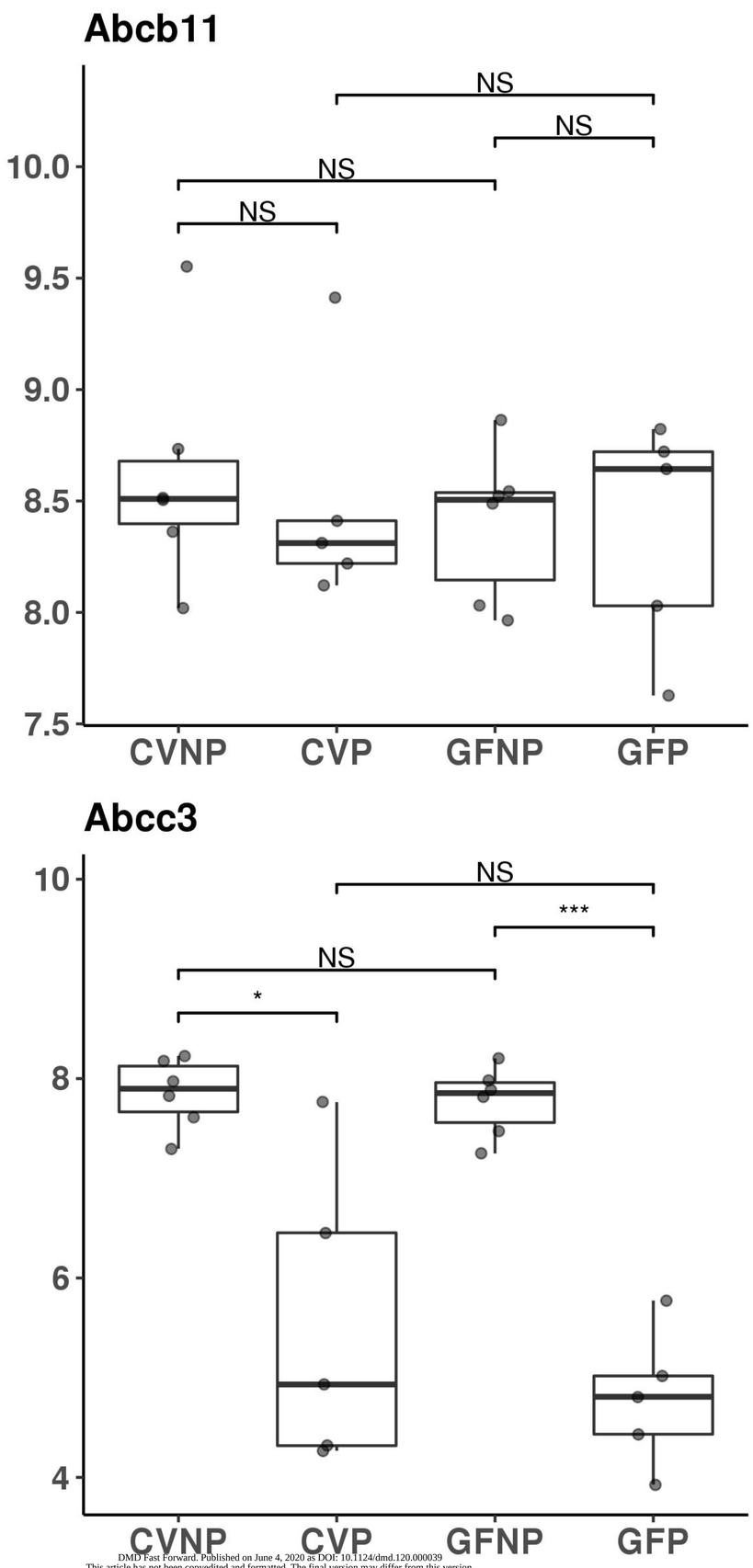

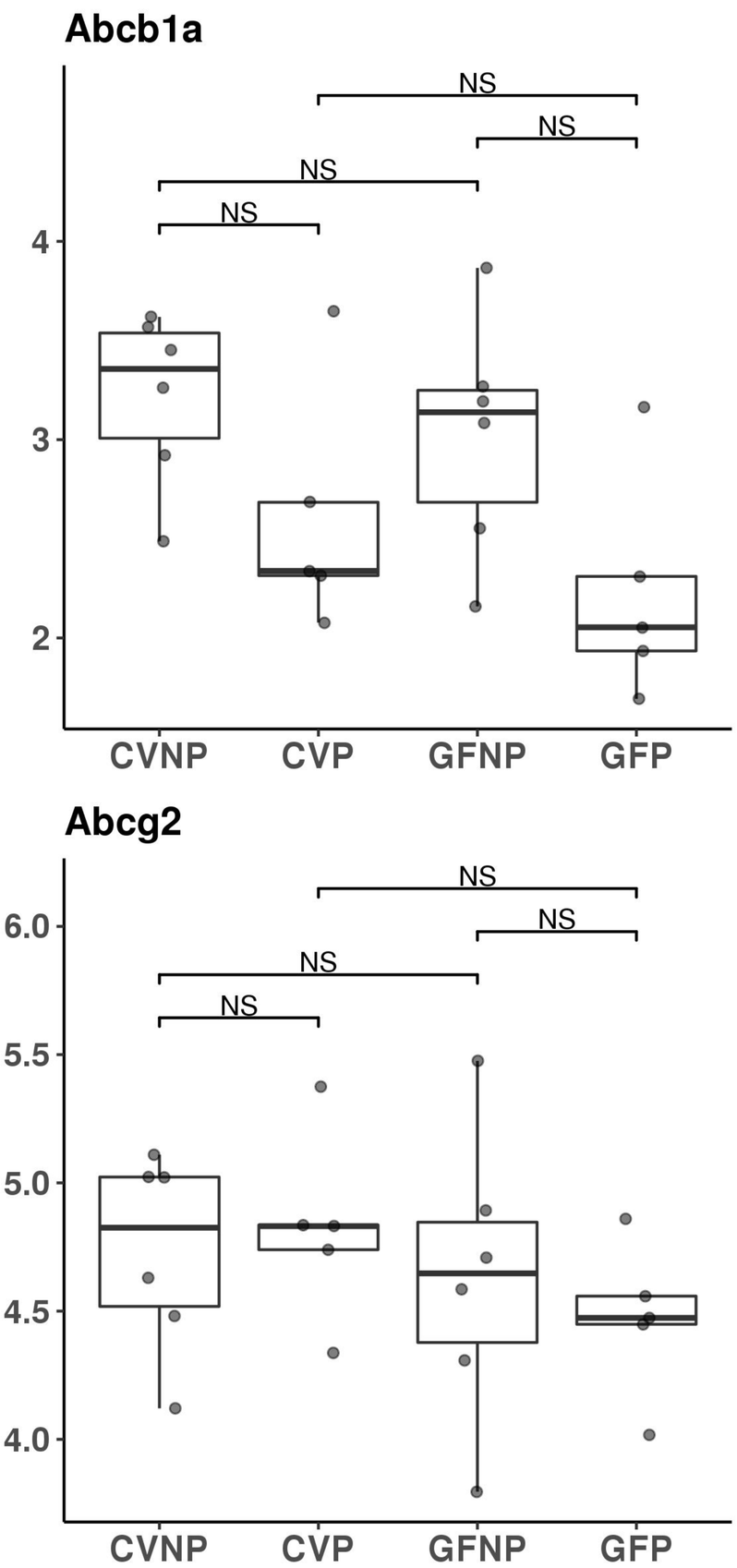

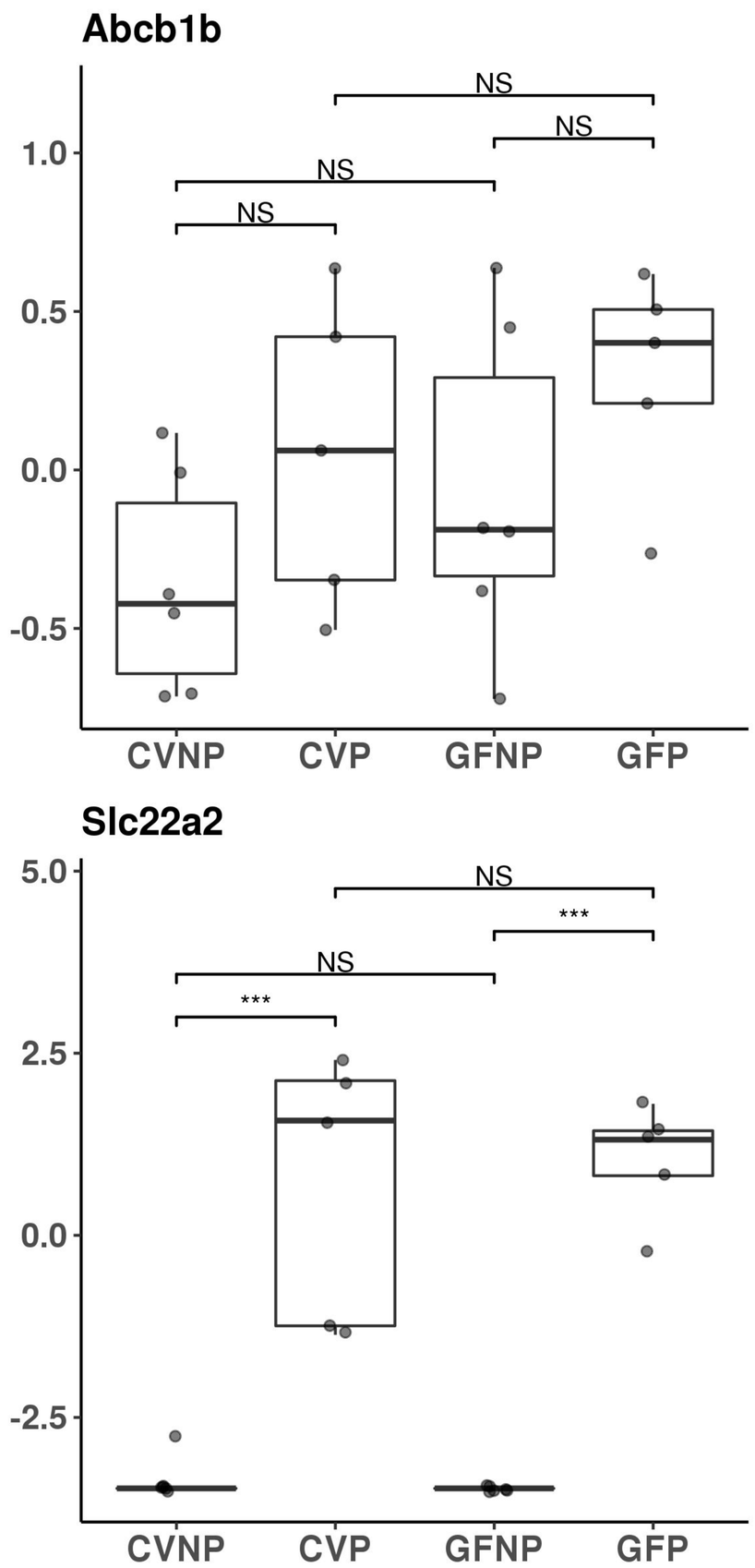

Log2 counts-per-million

DMD Fast Forward. Published on June 4, 2020 as DOI: 10.1124/dmd.120.000039

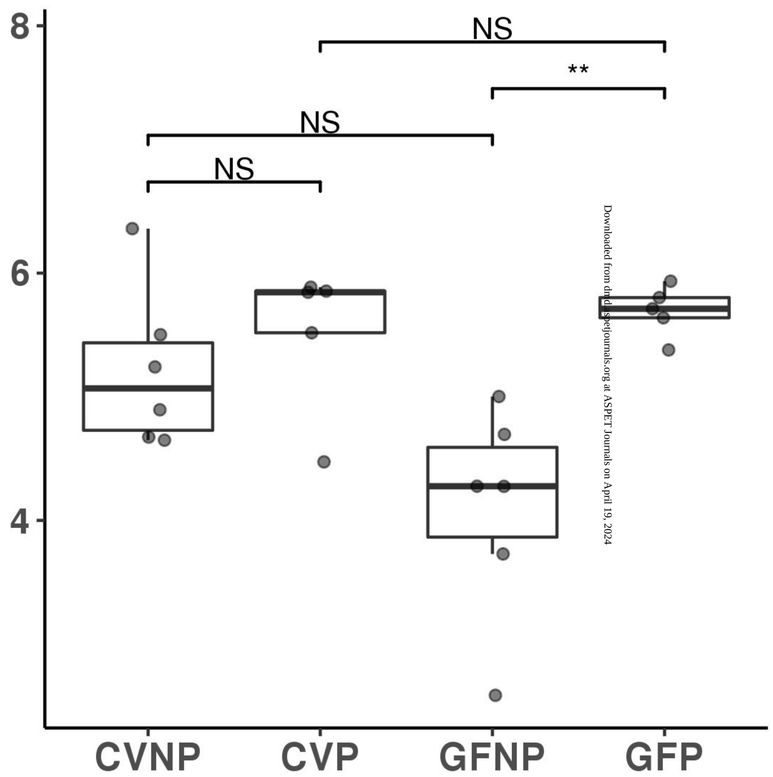

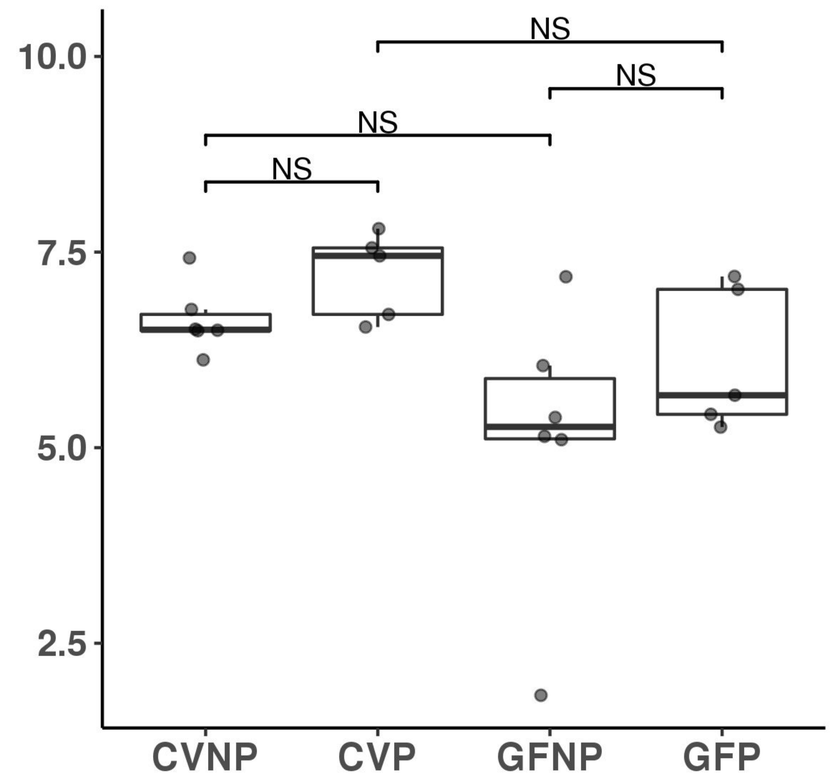

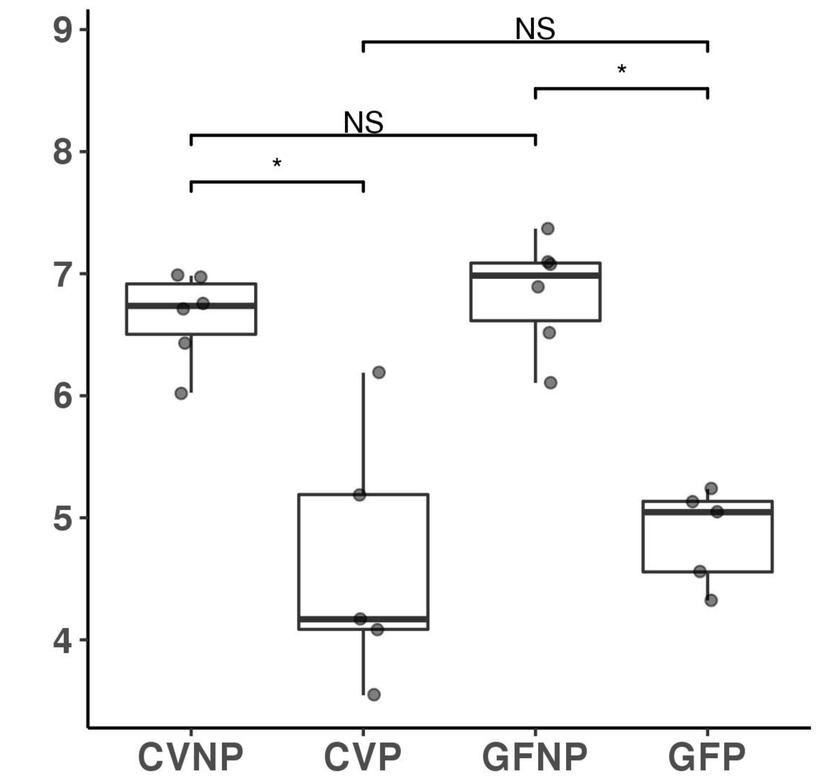

Figure 5

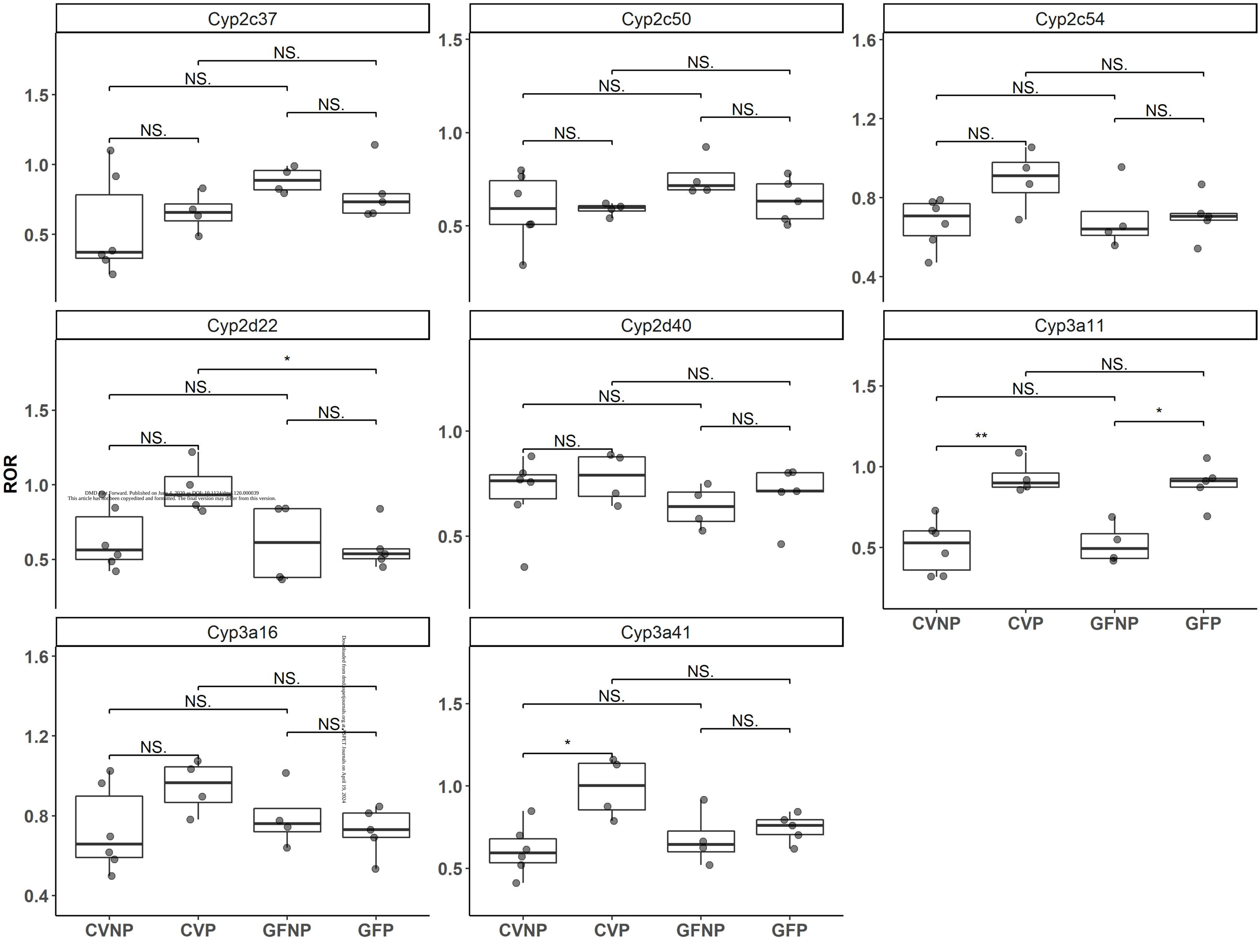

Figure 6

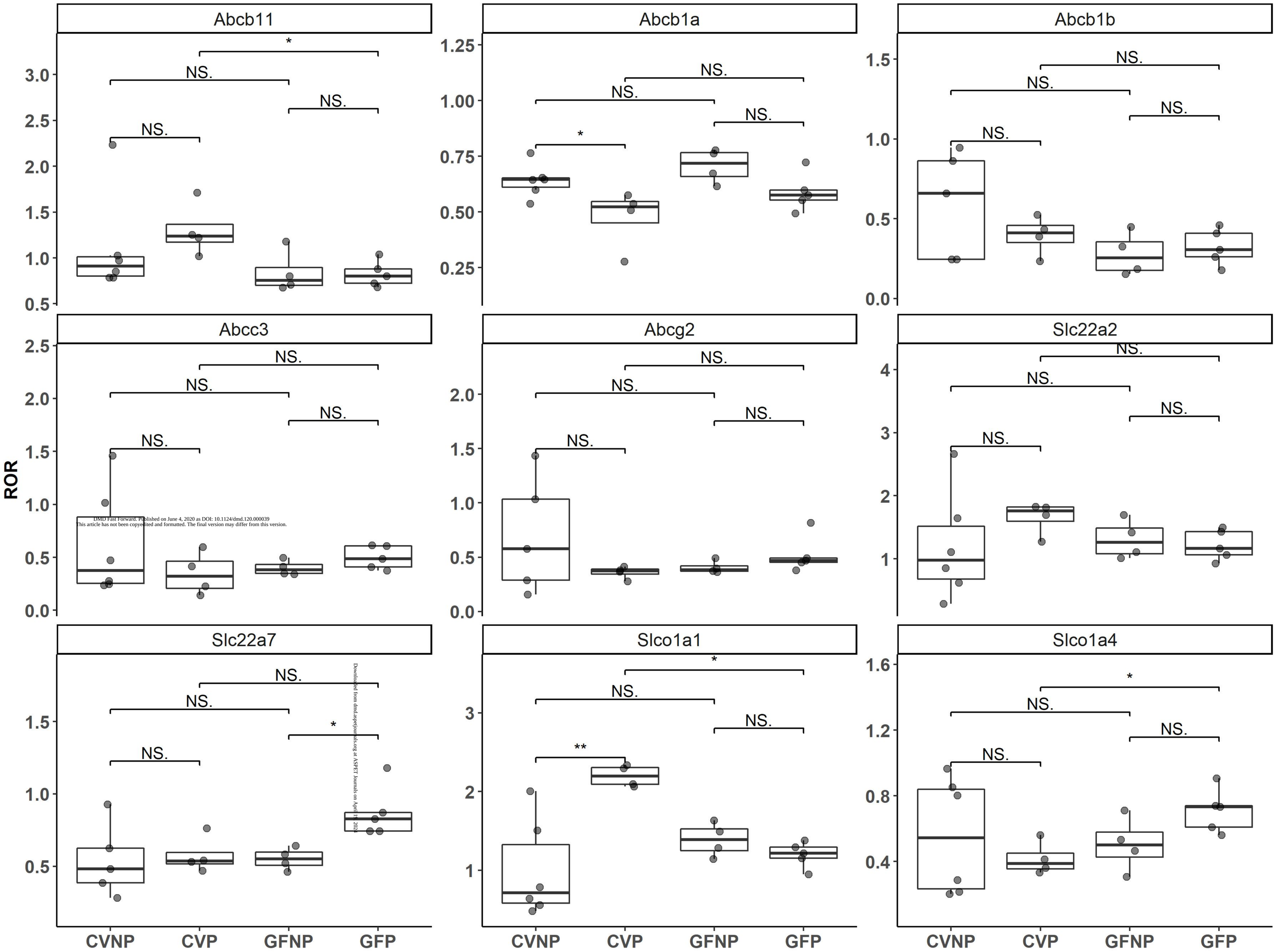

Figure 7

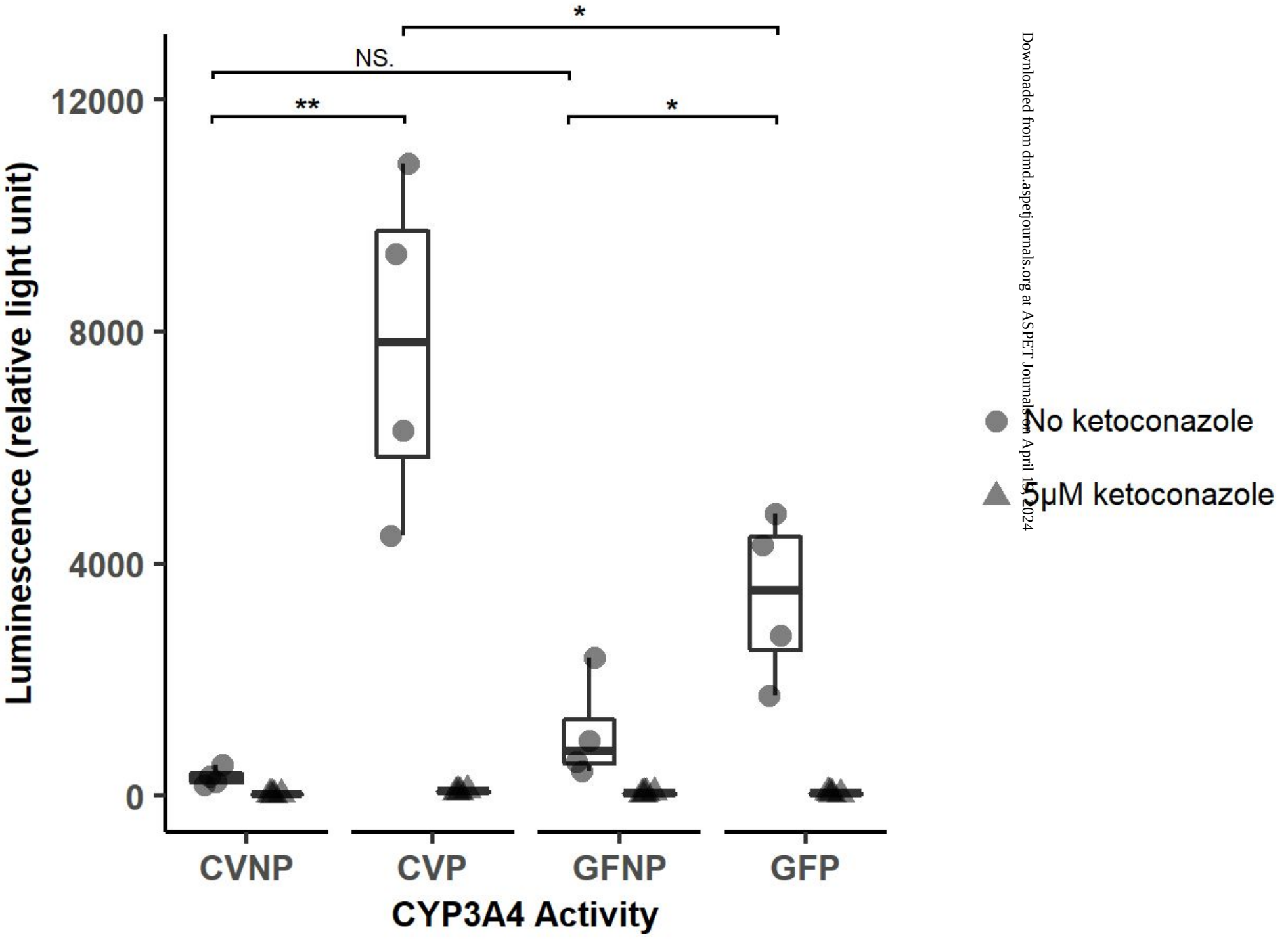

Figure 8

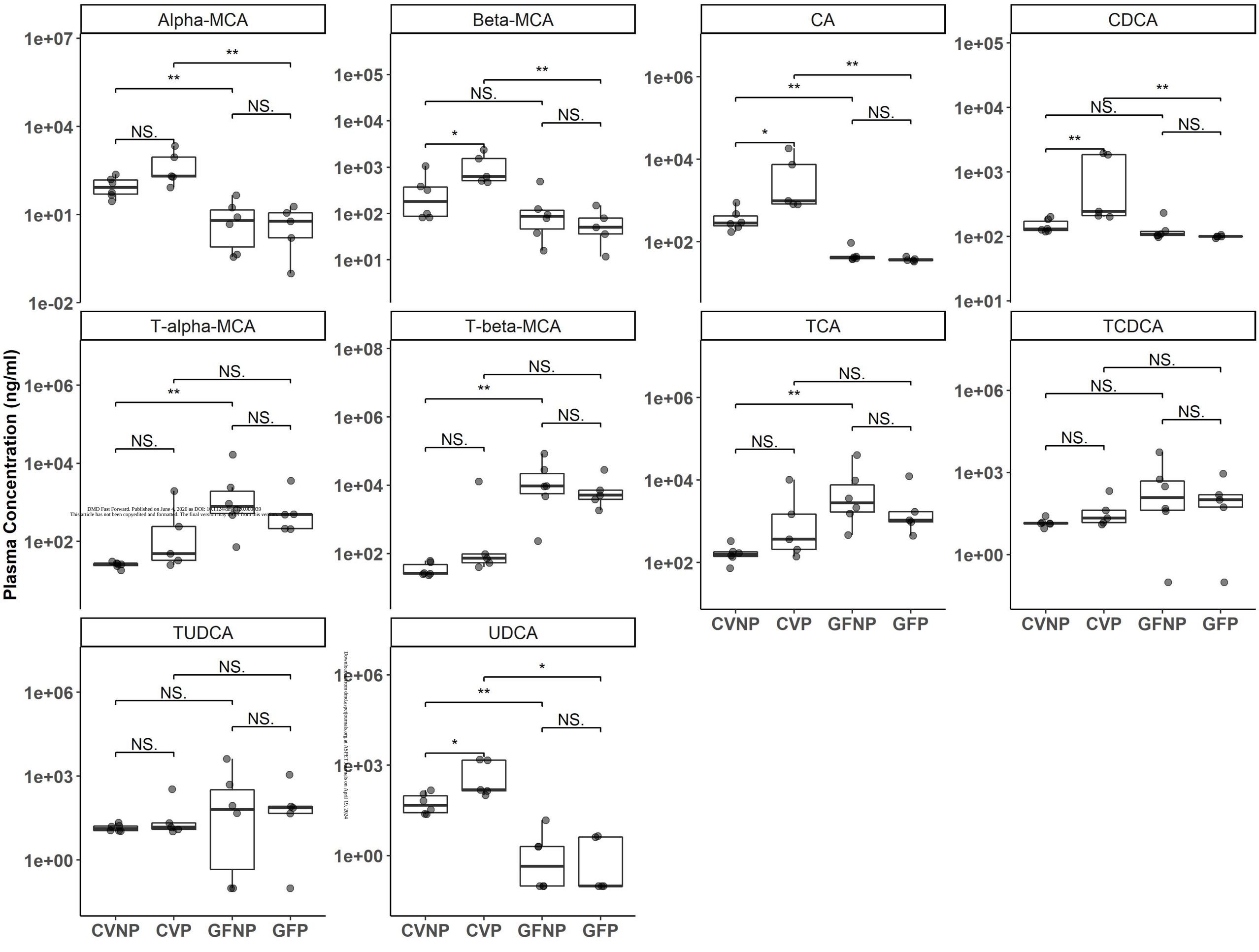

Figure 9

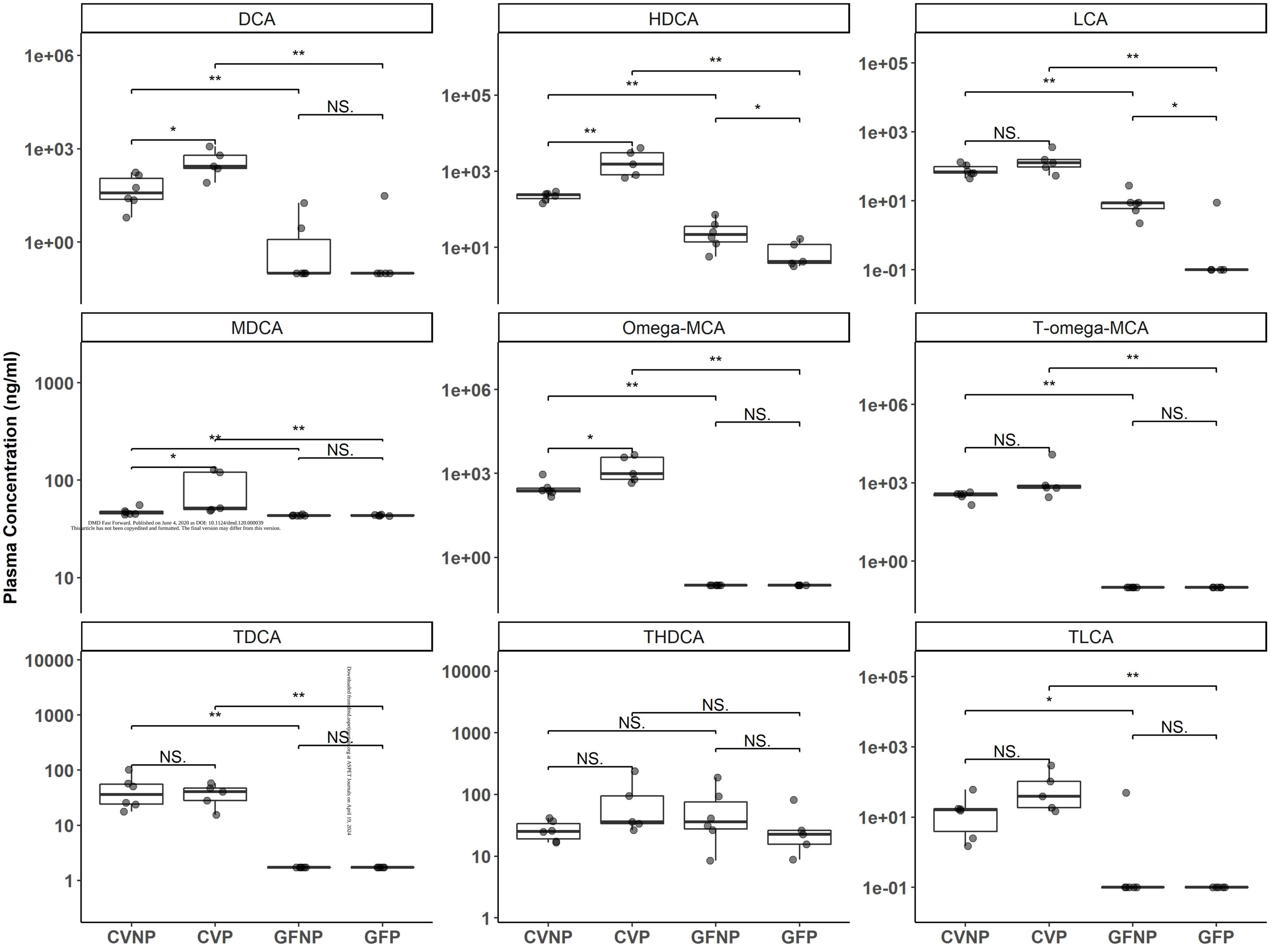

Figure 10

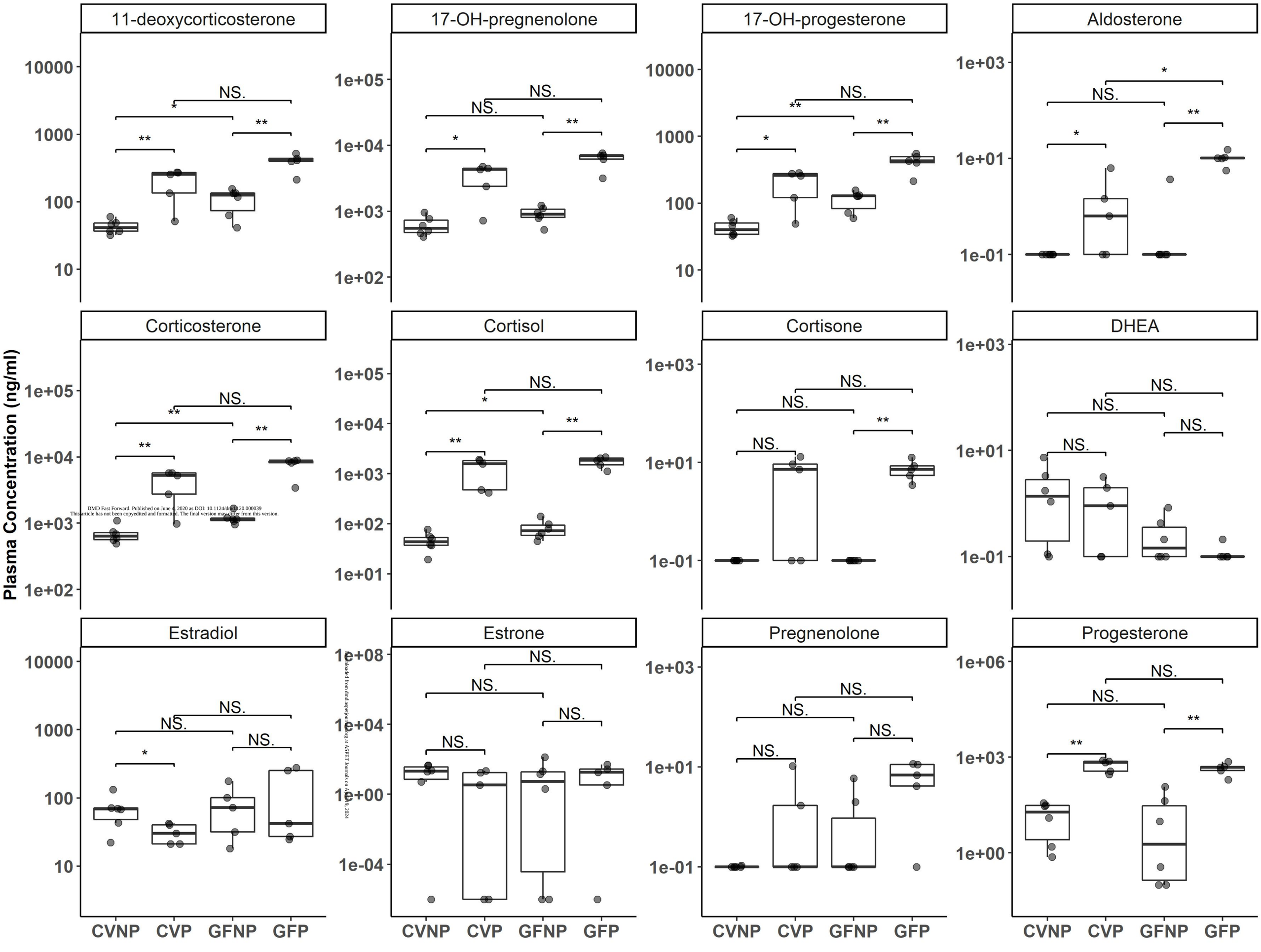

DMD-AR-2020-000039

Drug Metabolism and Disposition

Impact of Microbiome on Hepatic Metabolizing Enzymes and Transporters in Mice during Pregnancy

Lyrialle W. Han, Lu Wang, Yuanyuan Shi, Joseph L. Dempsey, Olesya V. Pershutkina, Moumita Dutta, Theo K. Bammler, Julia Y. Cui, and Qingcheng Mao

Supplemental Table S1. Surrogate peptides of cytochrome P450s and transporters and their MS/MS parameters for detection

Protein Name	Surrogate Peptide	Peptide Type	Parent Ion (m/z)	Fragment Ion (m/z)
Cyp2c37	DICQSFTNLSK	Light	656.8	796.4
Cyp2c37	DICQSFTNLSK	Light	656.8	709.4
Cyp2c50	YAILLLLK	Light	473.8	712.5
Cyp2c50	YAILLLLK	Light	473.8	599.4
Cyp2c54	ATNGMGIGFSNGSVWK	Light	813.4	1151.6
Cyp2c54	ATNGMGIGFSNGSVWK	Light	813.4	1094.6
Cyp2c54	ESLDVTIPR	Light	343.9	407.2
Cyp2c54	ESLDVTIPR	Light	343.9	350.7
Cyp2d22	MPYTNAVIHEVQR	Light	390.2	476.3
Cyp2d22	MPYTNAVIHEVQR	Light	390.2	476.2
Cyp2d40	GNPESSFNEANLR	Light	717.8	950.5
Cyp2d40	GNPESSFNEANLR	Light	717.8	863.4
Cyp3a11	ALLSPTFTSGK	Light	561.3	937.5
Cyp3a11	ALLSPTFTSGK	Light	561.3	824.4
Cyp3a11	ALLSPTFTSGK	Light	561.3	737.4
Cyp3a16	QDFFPVGIMSK	Light	423.5	731.4
Cyp3a16	QDFFPVGIMSK	Light	423.5	366.2
Cyp3a41	VDFLQLMMNAHNNSK	Light	441.2	599.3
Cyp3a41	VDFLQLMMNAHNNSK	Light	441.2	516.6
Cyp3a41	LQEEIDETLPNK	Light	476.9	701.4
Cyp3a41	LQEEIDETLPNK	Light	476.9	572.3
Cyp3a41	LQEEIDETLPNK	Light	476.9	120.1
BSA	LVNELTEFAK	Light	582.3	708.4
BSA	LVNELTEFAK	Light	582.3	951.5
BSA	AEFVEVTK	Light	461.7	722.4
BSA	AEFVEVTK	Light	461.7	347.2
BSA	AEFVEVTK	Heavy	465.8	859.5
BSA	AEFVEVTK	Heavy	465.8	730.4
BSA	AEFVEVTK	Heavy	465.8	583.4
BSA	AEFVEVTK	Heavy	465.8	484.3
Abcc3	HIFDQVIGPEGVLAGK	Light	840.5	1429.8
Abcc3	HIFDQVIGPEGVLAGK	Light	840.5	1282.7

Abcc3	HIFDQVIGPEGVLAGK	Heavy	844.5	1437.8
Abcc3	HIFDQVIGPEGVLAGK	Heavy	844.5	1290.7
Abcc3	HIFDQVIGPEGVLAGK	Heavy	844.5	1175.7
Abcc3	HIFDQVIGPEGVLAGK	Heavy	844.5	948.6
Abcc3	HIFDQVIGPEGVLAGK	Heavy	844.5	778.5
Abcb11	LSTALSGLLLGFYR	Light	504.3	655.4
Abcb11	LSTALSGLLLGFYR	Light	504.3	699.3
Abcb11	LSTALSGLLLGFYR	Light	504.3	605.4
Abcb11	FYDPCEGMVTLDGHDIR	Light	507.0	825.4
Abcb11	FYDPCEGMVTLDGHDIR	Light	507.0	712.3
Abcb11	FYDPCEGMVTLDGHDIR	Light	507.0	597.3
Abcg2	GEKPVIENLSEFYINSAIYGETK	Light	867.8	982.5
Abcg2	GEKPVIENLSEFYINSAIYGETK	Light	867.8	989.5
Mdr1a	ATVSASHIIR	Light	527.8	983.6
Mdr1a	ATVSASHIIR	Light	527.8	783.4
Mdr1b	GIYFSMVQAGAK	Light	636.3	791.4
Mdr1b	GIYFSMVQAGAK	Light	636.3	704.4
Slco1a1	YLEQQYGK	Light	514.8	623.3
Slco1a1	YLEQQYGK	Light	514.8	662.3
Slco1a1	YLEQQYGK	Heavy	518.8	873.5
Slco1a1	YLEQQYGK	Heavy	518.8	631.3
Slco1a1	YLEQQYGK	Heavy	518.8	662.3
Slc22a2	YEVDWNQSTLDCVDPLSSLAANR	Light	885.1	1043.5
Slc22a2	YEVDWNQSTLDCVDPLSSLAANR	Light	885.1	1131.5
Slc22a2	YEVDWNQSTLDCVDPLSSLAANR	Heavy	889.1	1043.5
Slc22a2	YEVDWNQSTLDCVDPLSSLAANR	Heavy	889.1	928.5
Slc22a2	LNPSFLDLVR	Light	587.3	946.5
Slc22a2	LNPSFLDLVR	Light	587.3	473.8
Slc22a2	LNPSFLDLVR	Heavy	592.3	956.5
Slc22a2	LNPSFLDLVR	Heavy	592.3	859.5
Slc22a2	LNPSFLDLVR	Heavy	592.3	772.4
Slc22a2	LNPSFLDLVR	Heavy	592.3	625.3
Slc22a2	LNPSFLDLVR	Heavy	592.3	478.8
Slc22a7	WLLLAATLPCVPGIISIWWVPESAR	Light	950.2	1343.7
Slc22a7	WLLLAATLPCVPGIISIWWVPESAR	Light	950.2	1230.6
Slco1a4	MYDINSFR	Light	349.2	409.2
Slco1a4	MYDINSFR	Light	349.2	457.7
Slco1a4	MYDINSFR	Light	349.2	376.2

Supplemental Table S2. Pregnancy and microbiome alter the mRNA expression of DMETs in female C57BL/6 livers. This list of genes was generated by comparing mRNA expression in groups between CVP and CVNP, GFP and GFNP, GFNP and CVNP, and GFP and CVP.

Gene Symbol	CVP vs. CVNP		GFP vs. GFNP		GFNP vs. CVNP		GFP vs. CVP	
	Fold Change	*FDR*	Fold Change	*FDR*	Fold Change	*FDR*	Fold Change	*FDR*
Cyp11a1	1.0	1.000	0.4	0.505	1.6	1.000	0.6	0.968
Cyp11b1	1.0	1.000	0.4	0.628	2.8	1.000	1.0	1.000
Cyp17a1	1.7	0.280	2.9	0.010	0.9	1.000	1.6	0.704
Cyp1a1	0.4	0.088	0.7	0.570	1.0	1.000	1.8	0.635
Cyp1a2	0.6	0.322	0.8	0.594	1.0	1.000	1.2	0.930
Cyp1b1	1.1	0.959	1.9	0.462	1.0	1.000	1.7	0.859
Cyp20a1	0.9	0.702	0.9	0.738	0.9	1.000	0.9	0.941
Cyp21a1	2.5	0.729	0.7	0.896	2.7	1.000	0.8	1.000
Cyp21a2-ps	0.7	0.797	0.9	0.932	0.8	1.000	1.0	1.000
Cyp24a1	1.0	1.000	1.0	1.000	1.0	1.000	1.0	1.000
Cyp26a1	3.2	0.076	4.2	0.020	0.9	1.000	1.1	0.996
Cyp26b1	0.0	<0.001	0.1	<0.001	1.9	0.982	5.0	0.289
Cyp26c1	0.8	0.920	0.7	0.814	0.8	1.000	0.7	0.969
Cyp27a1	0.5	0.077	0.6	0.121	0.7	1.000	0.8	0.857
Cyp2a12	1.0	0.975	1.3	0.641	1.0	1.000	1.4	0.824
Cyp2a21-ps	1.6	0.693	1.9	0.484	1.1	1.000	1.3	0.965
Cyp2a22	0.7	0.466	0.7	0.531	1.8	0.811	2.0	0.467
Cyp2a4	2.2	0.052	1.5	0.323	0.7	1.000	0.5	0.413
Cyp2a5	0.6	0.381	0.6	0.436	1.1	1.000	1.2	0.985
Cyp2ab1	0.5	0.709	0.6	0.813	1.2	1.000	1.7	0.969
Cyp2b10	1.2	0.828	0.8	0.837	1.0	1.000	0.6	0.840
Cyp2b13	0.1	<0.001	0.3	<0.001	1.2	1.000	5.3	<0.001
Cyp2b9	0.6	0.136	1.0	0.992	0.8	1.000	1.3	0.799
Cyp2c23	0.7	0.504	0.9	0.874	1.1	1.000	1.4	0.768
Cyp2c29	0.7	0.261	0.7	0.241	1.4	0.953	1.4	0.639
Cyp2c37	0.3	0.002	0.6	0.152	1.0	1.000	1.8	0.401
Cyp2c38	0.4	0.007	1.0	0.965	1.3	1.000	3.0	0.013
Cyp2c39	1.0	0.983	2.4	0.022	1.1	1.000	2.7	0.154
Cyp2c40	0.6	0.141	0.9	0.900	0.8	1.000	1.2	0.902
Cyp2c50	0.2	<0.001	0.5	0.001	1.0	1.000	2.0	0.066
Cyp2c54	0.4	0.001	0.8	0.561	1.0	1.000	2.2	0.074
Cyp2c55	0.5	0.216	0.1	<0.001	2.8	0.319	0.8	0.974
Cyp2c67	0.4	0.012	0.6	0.279	1.4	1.000	2.3	0.238
Cyp2c68	0.7	0.527	1.1	0.930	0.9	1.000	1.3	0.841
Cyp2c69	1.0	0.998	2.6	0.020	0.6	0.982	1.6	0.708
Cyp2c70	1.9	0.317	2.3	0.162	0.9	1.000	1.0	1.000

Cyp2d10	0.8	0.540	1.2	0.566	0.9	1.000	1.4	0.729
Cyp2d12	0.9	0.965	0.5	0.204	1.4	1.000	0.8	0.912
Cyp2d22	0.7	0.249	0.7	0.250	1.2	1.000	1.2	0.884
Cyp2d26	0.8	0.658	1.2	0.711	1.0	1.000	1.5	0.689
Cyp2d34	1.0	0.993	0.7	0.641	1.3	1.000	1.0	1.000
Cyp2d35-ps	1.6	0.742	0.9	0.934	2.2	1.000	1.2	0.995
Cyp2d36-ps	2.1	0.280	2.3	0.175	1.0	1.000	1.1	1.000
Cyp2d37-ps	1.6	0.342	1.2	0.754	1.0	1.000	0.8	0.898
Cyp2d38-ps	2.2	0.088	1.8	0.241	1.1	1.000	0.9	0.977
Cyp2d40	3.9	<0.001	5.4	<0.001	0.7	1.000	1.0	1.000
Cyp2d41-ps	1.2	0.831	0.9	0.907	1.0	1.000	0.7	0.904
Cyp2d9	0.3	0.025	0.2	0.002	1.8	1.000	1.1	1.000
Cyp2e1	0.4	0.141	0.7	0.474	1.1	1.000	1.6	0.799
Cyp2f2	0.6	0.182	0.8	0.507	0.7	1.000	0.9	0.977
Cyp2g1	2.8	0.047	3.6	0.010	0.6	1.000	0.8	0.964
Cyp2j5	0.8	0.627	0.9	0.901	1.0	1.000	1.1	0.985
Cyp2j6	0.8	0.543	1.1	0.808	0.9	1.000	1.3	0.774
Cyp2j9	0.4	0.153	0.4	0.103	0.8	1.000	0.7	0.894
Cyp2r1	1.0	0.962	1.2	0.622	0.6	0.439	0.7	0.722
Cyp2s1	0.3	0.222	4.5	0.072	0.5	1.000	7.1	0.238
Cyp2u1	0.8	0.720	0.9	0.902	0.7	1.000	0.8	0.869
Cyp39a1	0.4	0.031	0.3	0.017	1.0	1.000	0.9	0.999
Cyp3a11	0.6	0.290	0.3	0.005	0.6	0.953	0.3	0.131
Cyp3a13	1.0	1.000	1.6	0.478	0.9	1.000	1.5	0.874
Cyp3a16	20.6	0.001	128.0	<0.001	0.2	0.578	1.4	0.953
Cyp3a25	0.7	0.235	0.8	0.374	0.7	0.873	0.8	0.762
Cyp3a41a	4.8	0.047	10.8	0.002	0.6	1.000	1.4	0.941
Cyp3a41b	74.2	<0.001	181.7	<0.001	0.5	1.000	1.3	0.989
Cyp3a44	14.3	<0.001	30.5	<0.001	0.8	1.000	1.7	0.816
Cyp3a59	1.4	0.352	1.1	0.802	0.7	0.953	0.6	0.321
Cyp3a63-ps	5.1	0.047	8.5	0.007	0.9	1.000	1.5	0.926
Cyp46a1	0.6	0.547	0.4	0.117	1.0	1.000	0.6	0.816
Cyp4a10	0.7	0.494	0.8	0.721	1.2	1.000	1.4	0.782
Cyp4a12a	1.0	1.000	0.2	0.239	1.5	1.000	0.3	0.756
Cyp4a14	0.4	0.021	0.3	0.002	1.2	1.000	0.9	0.958
Cyp4a31	4.6	<0.001	5.3	<0.001	1.1	1.000	1.3	0.909
Cyp4a32	0.6	0.389	1.0	0.999	1.0	1.000	1.5	0.725
Cyp4b1	0.8	0.655	0.6	0.378	0.9	1.000	0.8	0.909
Cyp4f13	0.6	0.042	0.8	0.329	0.8	1.000	1.1	0.987
Cyp4f14	0.8	0.624	1.0	0.925	0.9	1.000	1.1	0.977
Cyp4f15	0.5	0.033	0.5	0.052	1.0	1.000	1.1	0.976
Cyp4f16	1.0	0.976	0.7	0.364	0.9	1.000	0.6	0.553
Cyp4f17	0.9	0.949	1.0	0.971	0.8	1.000	0.8	0.924
Cyp4f18	1.0	1.000	0.4	0.364	0.9	1.000	0.4	0.656
Cyp4v3	0.6	0.095	0.9	0.697	1.0	1.000	1.4	0.703
Cyp4x1	1.2	0.887	1.4	0.747	0.9	1.000	1.1	1.000
Cyp51	0.7	0.477	1.4	0.486	0.5	0.359	0.9	0.999
Cyp7a1	1.1	0.883	1.4	0.614	0.9	1.000	1.1	0.993

Cyp7b1	1.3	0.732	2.2	0.064	0.6	1.000	1.1	0.981
Cyp8b1	1.4	0.751	2.9	0.123	0.2	0.145	0.4	0.546
Ugt1a1	0.8	0.784	1.2	0.770	1.0	1.000	1.5	0.828
Ugt1a10	0.9	0.977	9.6	0.004	0.2	0.439	2.4	0.689
Ugt1a2	0.4	0.681	0.8	0.920	0.7	1.000	1.3	1.000
Ugt1a5	2.6	0.062	3.3	0.016	0.5	0.949	0.7	0.833
Ugt1a6a	1.3	0.698	1.3	0.674	0.9	1.000	0.9	0.976
Ugt1a6b	0.3	0.042	0.3	0.023	1.0	1.000	0.9	0.999
Ugt1a7c	0.8	0.893	1.8	0.449	0.8	1.000	1.8	0.799
Ugt1a8	0.3	0.496	0.2	0.230	2.9	1.000	1.6	0.974
Ugt1a9	0.9	0.970	1.8	0.237	1.1	1.000	2.1	0.440
Ugt2a2	0.7	0.836	0.9	0.938	0.9	1.000	1.1	1.000
Ugt2a3	0.8	0.364	0.9	0.869	0.9	1.000	1.1	0.943
Ugt2b1	0.8	0.435	0.8	0.360	1.2	1.000	1.1	0.924
Ugt2b34	0.8	0.709	0.9	0.884	0.9	1.000	1.1	1.000
Ugt2b35	1.3	0.522	1.2	0.648	0.9	1.000	0.9	0.954
Ugt2b36	1.2	0.815	1.5	0.447	1.1	1.000	1.4	0.833
Ugt2b37	0.7	0.800	0.8	0.876	0.5	1.000	0.5	0.797
Ugt2b38	0.2	0.139	0.0	0.013	0.5	1.000	0.1	0.408
Ugt2b5	0.9	0.841	0.9	0.799	1.1	1.000	1.0	1.000
Ugt3a1	0.7	0.510	1.0	0.973	1.0	1.000	1.4	0.809
Ugt3a2	0.9	0.957	1.4	0.579	0.9	1.000	1.3	0.915
Ugt8a	0.9	0.968	1.0	0.998	2.5	1.000	2.7	0.764
Sult1a1	0.9	0.863	1.1	0.936	1.3	1.000	1.6	0.769
Sult1b1	1.2	0.761	1.4	0.428	1.3	1.000	1.5	0.690
Sult1c2	1.0	0.981	2.1	0.067	0.9	1.000	1.9	0.467
Sult1d1	0.3	0.277	0.4	0.342	1.4	1.000	1.7	0.916
Sult1e1	0.2	0.417	0.2	0.255	9.9	0.411	13.6	0.454
Sult2a1	1.1	0.966	1.5	0.801	0.4	1.000	0.6	0.938
Sult2a2	0.6	0.750	0.5	0.557	1.0	1.000	0.8	0.989
Sult2a3	0.5	0.697	0.2	0.239	1.7	1.000	0.6	0.975
Sult2a5	0.2	0.122	0.2	0.066	1.0	1.000	0.7	0.978
Sult2a7	0.2	0.061	0.2	0.031	0.9	1.000	0.7	0.964
Sult2a8	1.1	0.934	1.5	0.548	0.9	1.000	1.2	0.982
Sult2b1	3.9	0.440	2.3	0.415	8.6	0.555	5.0	0.412
Sult3a1	3.6	0.056	12.9	<0.001	0.3	0.359	1.0	1.000
Sult3a2	53.9	<0.001	226.7	<0.001	0.2	0.605	0.9	1.000
Sult4a1	287.7	<0.001	3.5	0.333	5.2	1.000	0.1	0.129
Sult5a1	0.7	0.632	0.5	0.291	0.2	0.134	0.1	0.081
Gsta1	7.4	0.160	0.1	0.086	9.5	0.564	0.1	0.444
Gsta2	0.6	0.215	0.4	0.033	2.0	0.605	1.5	0.782
Gsta3	0.9	0.942	1.0	0.964	0.9	1.000	1.0	1.000
Gsta4	0.5	0.181	0.5	0.098	1.2	1.000	1.1	0.989
Gstcd	1.6	0.311	1.0	0.966	1.0	1.000	0.7	0.763
Gstk1	0.5	0.005	0.5	0.018	1.1	1.000	1.2	0.901
Gstm1	1.0	0.984	0.7	0.498	1.1	1.000	0.7	0.838
Gstm2	1.8	0.041	1.4	0.248	1.4	1.000	1.1	0.984
Gstm3	3.1	0.044	0.6	0.456	2.5	0.564	0.5	0.625

Gstm4	1.1	0.800	0.8	0.503	0.8	1.000	0.5	0.289
Gstm5	1.1	0.948	1.2	0.635	0.7	1.000	0.8	0.884
Gstm6	0.9	0.908	0.9	0.892	1.3	1.000	1.3	0.922
Gstm7	0.8	0.809	0.8	0.797	1.0	1.000	1.1	1.000
Gsto1	0.8	0.496	1.1	0.882	0.9	1.000	1.3	0.822
Gsto2	1.0	1.000	1.1	0.938	0.5	1.000	0.6	0.817
Gstp1	3.4	0.002	2.2	0.039	0.9	1.000	0.6	0.635
Gstp2	5.9	0.016	1.8	0.505	0.9	1.000	0.3	0.386
Gstp3	1.9	0.190	1.4	0.516	1.1	1.000	0.8	0.951
Gstt1	0.4	0.005	0.4	0.017	0.8	1.000	0.9	0.976
Gstt2	0.6	0.182	0.7	0.380	0.9	1.000	1.0	1.000
Gstt3	1.5	0.177	2.0	0.005	0.8	1.000	1.1	0.951
Abca1	1.3	0.494	1.4	0.365	1.0	1.000	1.0	1.000
Abca13	10.9	0.144	0.2	0.365	5.3	1.000	0.1	0.451
Abca17	103.3	<0.001	1779.0	<0.001	0.1	0.757	1.2	0.989
Abca2	1.2	0.873	1.4	0.579	0.8	1.000	1.0	1.000
Abca3	1.1	0.896	1.8	0.112	0.6	0.873	1.0	1.000
Abca4	2.0	0.383	0.7	0.702	1.1	1.000	0.4	0.526
Abca5	2.0	0.025	3.3	<0.001	0.8	1.000	1.3	0.768
Abca6	1.1	0.951	1.4	0.512	1.0	1.000	1.3	0.859
Abca7	0.9	0.851	0.5	0.006	1.1	1.000	0.6	0.298
Abca8a	0.7	0.493	0.5	0.158	1.4	1.000	1.0	1.000
Abca8b	1.2	0.650	1.4	0.308	0.9	1.000	1.1	0.999
Abca9	1.5	0.328	1.3	0.495	1.1	1.000	1.0	1.000
Abcb10	0.9	0.586	1.0	0.964	0.8	0.817	0.9	0.856
Abcb11	0.7	0.438	0.9	0.794	0.9	1.000	1.2	0.950
Abcb1a	0.6	0.333	0.7	0.438	0.9	1.000	1.0	1.000
Abcb1b	1.7	0.553	1.8	0.465	1.2	1.000	1.2	0.986
Abcb4	0.6	0.214	0.7	0.424	0.9	1.000	1.0	1.000
Abcb6	0.6	0.019	0.7	0.129	1.0	1.000	1.2	0.830
Abcb7	1.0	0.939	1.3	0.387	0.8	1.000	1.0	1.000
Abcb8	0.6	0.057	0.6	0.091	0.9	1.000	1.0	1.000
Abcb9	1.2	0.650	1.0	0.973	1.2	1.000	1.0	1.000
Abcc1	1.6	0.344	0.9	0.890	1.6	0.978	0.9	0.998
Abcc10	0.8	0.667	0.7	0.303	1.1	1.000	0.9	0.985
Abcc12	0.8	0.840	0.5	0.456	0.9	1.000	0.6	0.876
Abcc2	0.8	0.803	0.8	0.768	1.0	1.000	1.0	1.000
Abcc3	0.3	0.025	0.1	<0.001	1.0	1.000	0.5	0.613
Abcc4	1.4	0.698	1.0	0.977	1.5	1.000	1.2	0.978
Abcc5	1.4	0.635	0.9	0.863	1.1	1.000	0.7	0.816
Abcc6	0.6	0.364	0.7	0.395	1.1	1.000	1.2	0.955
Abcc8	0.7	0.928	1.4	0.901	1.3	1.000	2.5	0.914
Abcc9	1.0	0.979	1.2	0.667	0.9	1.000	1.2	0.941
Abcd1	1.0	0.959	1.2	0.426	0.8	1.000	1.0	1.000
Abcd2	1.1	0.947	1.4	0.650	0.7	1.000	0.9	1.000
Abcd3	0.8	0.328	0.8	0.538	0.8	0.877	0.8	0.801
Abcd4	0.8	0.406	0.6	0.078	1.2	1.000	1.0	1.000
Abce1	1.1	0.715	1.2	0.477	1.0	1.000	1.0	1.000

Abcf1	0.9	0.652	1.0	0.983	0.9	1.000	1.0	1.000
Abcf2	0.9	0.817	1.0	0.893	0.9	1.000	1.0	0.997
Abcf3	0.7	0.151	0.8	0.377	0.8	1.000	0.9	0.988
Abcg1	1.3	0.734	0.9	0.880	0.9	1.000	0.7	0.773
Abcg2	1.1	0.762	1.1	0.800	0.9	1.000	0.9	0.969
Abcg3	1.5	0.459	1.0	0.975	0.9	1.000	0.6	0.678
Abcg4	3.2	0.693	0.4	0.581	9.4	0.917	1.1	1.000
Abcg5	0.4	0.003	0.4	0.009	1.3	1.000	1.4	0.696
Abcg8	0.5	0.008	0.6	0.061	1.2	1.000	1.4	0.613
Slc10a1	0.4	0.020	0.5	0.045	0.8	1.000	1.0	1.000
Slc10a2	0.9	0.947	1.2	0.693	1.0	1.000	1.3	0.878
Slc10a3	0.9	0.681	1.0	1.000	0.8	1.000	1.0	1.000
Slc10a5	1.2	0.821	1.1	0.915	0.9	1.000	0.8	0.972
Slc10a6	0.2	0.249	0.6	0.650	1.0	1.000	2.4	0.830
Slc10a7	1.0	0.978	0.8	0.495	1.3	1.000	1.0	1.000
Slc11a1	1.5	0.567	1.2	0.836	0.7	1.000	0.6	0.689
Slc11a2	1.4	0.314	0.9	0.855	1.0	1.000	0.7	0.514
Slc12a2	0.9	0.888	1.1	0.725	1.3	0.962	1.5	0.314
Slc12a3	0.8	0.900	0.7	0.697	1.7	1.000	1.4	0.945
Slc12a4	0.9	0.914	0.8	0.408	1.0	1.000	0.8	0.820
Slc12a5	0.7	0.792	0.5	0.446	0.9	1.000	0.7	0.916
Slc12a6	1.1	0.789	0.9	0.662	1.1	1.000	0.9	0.901
Slc12a7	0.6	0.153	0.6	0.066	0.8	1.000	0.8	0.768
Slc12a8	1.2	0.909	1.0	1.000	1.3	1.000	1.1	1.000
Slc12a9	0.7	0.472	0.9	0.883	1.1	1.000	1.4	0.768
Slc13a2	1.4	0.779	2.6	0.158	0.5	1.000	1.0	1.000
Slc13a3	0.4	0.068	0.5	0.244	0.7	1.000	0.9	0.997
Slc13a4	0.3	0.250	0.6	0.672	0.6	1.000	1.2	1.000
Slc13a5	0.4	0.216	0.2	0.070	0.8	1.000	0.5	0.788
Slc14a1	1.4	0.878	6.5	0.066	0.5	1.000	2.5	0.768
Slc14a2	1.4	0.947	3.9	0.479	0.2	1.000	0.5	0.941
Slc15a1	1.2	0.915	0.9	0.938	1.2	1.000	0.8	0.995
Slc15a2	1.5	0.736	0.3	0.229	2.3	1.000	0.5	0.809
Slc15a3	1.8	0.316	1.0	0.994	0.9	1.000	0.5	0.550
Slc15a4	0.9	0.761	0.6	0.072	1.2	1.000	0.8	0.874
Slc15a5	0.5	0.404	0.7	0.786	0.5	1.000	0.8	0.986
Slc16a1	2.0	0.018	1.6	0.142	0.9	1.000	0.7	0.625
Slc16a10	0.5	0.051	0.7	0.283	1.1	1.000	1.5	0.635
Slc16a11	0.9	0.897	1.0	0.995	0.6	0.953	0.7	0.768
Slc16a12	0.5	0.088	0.7	0.401	0.9	1.000	1.2	0.945
Slc16a13	2.2	0.136	1.6	0.408	0.5	0.940	0.4	0.347
Slc16a2	0.7	0.628	1.0	0.974	0.8	1.000	1.1	0.999
Slc16a3	3.3	0.107	1.1	0.959	2.2	1.000	0.7	0.945
Slc16a4	0.9	0.900	0.6	0.341	1.2	1.000	0.8	0.946
Slc16a5	1.0	0.978	1.2	0.781	1.1	1.000	1.2	0.917
Slc16a6	16.2	<0.001	14.4	<0.001	1.1	1.000	1.0	1.000
Slc16a7	0.7	0.458	0.8	0.633	1.1	1.000	1.2	0.854
Slc16a9	1.1	0.908	1.2	0.752	0.9	1.000	1.0	1.000

Slc17a1	0.7	0.687	0.6	0.507	1.0	1.000	0.9	0.993
Slc17a2	0.3	0.057	0.2	0.009	0.9	1.000	0.6	0.816
Slc17a3	0.7	0.336	0.9	0.685	0.9	1.000	1.1	0.987
Slc17a4	1.7	0.415	1.5	0.493	1.3	1.000	1.1	0.996
Slc17a5	0.9	0.930	1.1	0.872	1.0	1.000	1.2	0.930
Slc17a8	1.9	0.375	0.6	0.519	1.0	1.000	0.4	0.383
Slc17a9	1.4	0.593	1.2	0.757	0.9	1.000	0.8	0.950
Slc18a1	1.4	0.575	1.1	0.845	1.3	1.000	1.1	1.000
Slc18a2	1.0	0.977	1.0	0.984	1.0	1.000	0.9	1.000
Slc18b1	0.9	0.915	1.1	0.939	0.8	1.000	1.0	1.000
Slc19a1	0.6	0.178	0.8	0.557	1.1	1.000	1.4	0.761
Slc19a2	0.7	0.156	0.7	0.198	0.9	1.000	0.9	0.996
Slc19a3	0.4	0.650	3.7	0.483	0.4	1.000	3.7	0.816
Slc1a1	1.2	0.900	1.4	0.800	0.9	1.000	1.1	1.000
Slc1a2	1.5	0.699	2.1	0.313	1.4	1.000	2.0	0.756
Slc1a3	1.5	0.825	0.6	0.660	1.4	1.000	0.5	0.895
Slc1a4	1.8	0.140	1.0	1.000	1.1	1.000	0.6	0.533
Slc1a5	0.7	0.616	0.5	0.141	1.3	1.000	0.9	0.987
Slc1a6	0.5	0.714	0.3	0.475	0.9	1.000	0.5	0.951
Slc20a1	0.6	0.059	0.7	0.141	1.1	1.000	1.2	0.832
Slc20a2	1.4	0.188	1.5	0.113	1.0	1.000	1.0	1.000
Slc22a1	0.8	0.595	0.9	0.847	1.0	1.000	1.2	0.953
Slc22a13b-ps	0.4	0.487	0.5	0.528	0.9	1.000	1.0	1.000
Slc22a15	0.5	0.008	0.5	0.028	1.1	1.000	1.2	0.869
Slc22a17	1.0	0.990	0.9	0.906	0.9	1.000	0.8	0.975
Slc22a18	0.7	0.294	0.9	0.810	1.0	1.000	1.4	0.768
Slc22a2	260.5	<0.001	561.5	<0.001	0.4	1.000	0.8	0.984
Slc22a21	0.3	0.083	1.9	0.337	0.5	0.889	2.8	0.433
Slc22a23	1.4	0.270	1.6	0.080	1.0	1.000	1.1	0.967
Slc22a26	0.6	0.352	1.0	1.000	0.7	1.000	1.1	0.985
Slc22a27	0.5	0.126	0.5	0.101	0.6	0.992	0.6	0.665
Slc22a28	2.9	0.100	2.8	0.102	1.3	1.000	1.2	0.976
Slc22a29	0.2	0.075	0.2	0.072	0.9	1.000	0.9	1.000
Slc22a3	0.9	0.930	0.9	0.890	1.6	1.000	1.6	0.767
Slc22a30	1.1	0.852	1.3	0.317	0.9	1.000	1.1	0.996
Slc22a4	0.5	0.194	0.8	0.825	0.8	1.000	1.3	0.917
Slc22a5	0.8	0.566	0.9	0.709	1.0	1.000	1.1	0.951
Slc22a6	0.4	0.654	0.2	0.449	1.7	1.000	1.0	1.000
Slc22a7	1.3	0.713	3.1	0.004	0.5	0.437	1.1	0.975
Slc22a8	0.3	0.567	0.0	0.108	1.9	1.000	0.3	0.890
Slc23a1	1.0	1.000	1.2	0.682	0.7	1.000	0.9	0.969
Slc23a2	0.6	0.194	0.7	0.336	0.9	1.000	1.0	1.000
Slc23a3	1.1	0.975	0.6	0.764	2.7	1.000	1.5	0.974
Slc23a4	1.6	0.654	0.4	0.269	1.7	1.000	0.4	0.681
Slc24a3	9.5	<0.001	6.6	<0.001	1.3	1.000	0.9	0.969
Slc24a5	0.7	0.690	0.9	0.920	0.6	1.000	0.8	0.962
Slc25a1	0.7	0.153	0.8	0.343	0.7	0.811	0.8	0.786
Slc25a10	0.7	0.080	0.8	0.336	0.9	1.000	1.0	1.000

Slc25a11	0.7	0.016	0.7	0.029	1.0	1.000	1.0	1.000
Slc25a12	1.0	0.989	0.9	0.845	0.9	1.000	0.8	0.901
Slc25a13	0.7	0.220	0.8	0.529	1.0	1.000	1.2	0.880
Slc25a14	1.1	0.944	0.7	0.420	1.1	1.000	0.7	0.768
Slc25a15	0.8	0.688	0.9	0.833	1.3	1.000	1.4	0.713
Slc25a16	1.0	0.995	1.1	0.796	1.1	1.000	1.2	0.857
Slc25a17	1.0	0.943	0.9	0.500	0.9	1.000	0.8	0.654
Slc25a18	1.4	0.820	0.4	0.257	2.5	0.940	0.7	0.945
Slc25a19	0.8	0.291	0.6	0.015	1.1	1.000	0.9	0.857
Slc25a20	1.0	0.975	1.0	0.908	1.0	1.000	0.9	0.946
Slc25a21	0.7	0.286	0.6	0.182	1.0	1.000	0.9	0.978
Slc25a22	1.0	0.990	0.7	0.221	1.4	0.757	1.0	0.999
Slc25a23	0.7	0.245	1.0	1.000	0.8	1.000	1.2	0.924
Slc25a24	1.1	0.862	1.2	0.703	1.1	1.000	1.2	0.945
Slc25a25	1.1	0.885	1.1	0.861	1.6	1.000	1.6	0.701
Slc25a26	1.1	0.849	1.1	0.732	0.9	1.000	1.0	1.000
Slc25a27	0.8	0.836	0.4	0.229	1.8	1.000	1.0	1.000
Slc25a28	0.6	0.007	0.7	0.024	0.9	1.000	0.9	0.953
Slc25a29	0.8	0.585	1.0	0.977	1.0	1.000	1.3	0.816
Slc25a3	0.8	0.504	0.8	0.231	1.0	1.000	0.9	0.947
Slc25a30	1.7	0.128	2.2	0.010	0.5	0.315	0.7	0.639
Slc25a31	0.4	0.521	0.4	0.589	1.0	1.000	1.2	1.000
Slc25a32	0.8	0.457	0.8	0.381	1.3	1.000	1.3	0.722
Slc25a33	1.4	0.250	1.5	0.147	0.9	1.000	0.9	0.999
Slc25a34	1.0	1.000	1.1	0.936	1.0	1.000	1.1	0.998
Slc25a35	0.7	0.608	0.9	0.890	0.9	1.000	1.2	0.985
Slc25a36	1.2	0.683	1.5	0.299	1.1	1.000	1.3	0.837
Slc25a37	0.5	0.012	0.6	0.027	0.9	1.000	1.0	1.000
Slc25a38	0.9	0.631	0.9	0.609	1.1	1.000	1.1	0.869
Slc25a39	0.7	0.070	0.8	0.298	0.9	1.000	1.0	0.994
Slc25a4	1.0	0.948	0.8	0.628	1.0	1.000	0.8	0.799
Slc25a40	1.1	0.943	0.9	0.833	0.9	1.000	0.8	0.854
Slc25a42	0.8	0.396	0.7	0.320	0.9	1.000	0.9	0.912
Slc25a43	0.8	0.876	0.5	0.329	0.8	1.000	0.4	0.625
Slc25a44	1.1	0.895	1.1	0.701	1.0	1.000	1.0	1.000
Slc25a45	0.9	0.916	1.0	0.983	0.8	1.000	0.9	0.913
Slc25a46	0.9	0.787	1.1	0.728	1.0	1.000	1.2	0.800
Slc25a47	0.9	0.746	0.9	0.861	1.2	1.000	1.3	0.817
Slc25a48	0.6	0.189	0.7	0.387	1.2	1.000	1.4	0.753
Slc25a5	0.8	0.388	0.8	0.271	0.9	1.000	0.9	0.886
Slc25a51	0.6	0.026	0.3	<0.001	1.8	0.181	1.1	0.951
Slc25a53	1.2	0.893	0.7	0.703	1.4	1.000	0.8	0.979
Slc26a1	0.8	0.793	1.1	0.903	0.9	1.000	1.1	0.988
Slc26a10	0.4	0.079	0.3	0.006	1.3	1.000	0.9	0.988
Slc26a11	0.9	0.864	0.7	0.206	1.1	1.000	0.8	0.833
Slc26a2	1.2	0.580	1.0	0.994	1.1	1.000	0.9	0.961
Slc26a3	1.4	0.899	7.5	0.104	0.9	1.000	4.8	0.601
Slc26a4	0.1	0.009	0.2	0.016	1.2	1.000	1.6	0.947

Slc26a6	1.1	0.955	1.9	0.062	0.5	0.536	1.0	1.000
Slc26a7	0.1	0.150	3.3	0.516	0.1	0.615	3.3	0.838
Slc26a8	0.4	0.450	0.7	0.800	0.9	1.000	1.6	0.950
Slc27a1	0.7	0.210	0.6	0.018	1.3	1.000	1.0	1.000
Slc27a2	0.7	0.547	0.7	0.530	1.0	1.000	1.0	1.000
Slc27a3	1.9	0.334	0.8	0.754	2.7	0.438	1.1	0.998
Slc27a4	1.0	0.934	1.2	0.517	0.9	1.000	1.1	0.945
Slc27a5	0.6	0.242	0.9	0.837	0.8	1.000	1.2	0.943
Slc27a6	1.8	0.632	0.8	0.920	1.5	1.000	0.7	0.951
Slc28a1	0.4	0.347	0.6	0.572	0.8	1.000	1.2	1.000
Slc28a2	1.3	0.804	1.3	0.788	1.0	1.000	1.0	1.000
Slc28a3	0.4	0.702	0.7	0.837	4.2	0.875	7.3	0.597
Slc29a1	0.7	0.137	0.7	0.166	1.1	1.000	1.2	0.888
Slc29a2	0.6	0.285	0.4	0.075	1.0	1.000	0.7	0.888
Slc29a3	1.2	0.806	1.5	0.321	0.8	1.000	1.1	0.993
Slc29a4	0.9	0.996	0.2	0.287	2.8	1.000	0.7	0.983
Slc2a1	1.0	0.990	0.9	0.940	0.9	1.000	0.8	0.946
Slc2a10	0.9	0.977	1.4	0.800	0.8	1.000	1.2	0.999
Slc2a12	0.7	0.737	3.2	0.106	0.4	0.761	1.6	0.847
Slc2a13	1.3	0.817	0.6	0.495	1.9	0.995	1.0	1.000
Slc2a2	0.5	0.233	0.6	0.438	1.1	1.000	1.4	0.911
Slc2a3	1.9	0.495	3.4	0.116	2.8	0.873	5.0	0.242
Slc2a4	0.3	0.257	0.4	0.296	2.0	1.000	2.3	0.739
Slc2a4rg-ps	0.6	0.453	0.4	0.071	1.2	1.000	0.8	0.914
Slc2a5	0.9	0.948	1.2	0.796	0.9	1.000	1.1	0.991
Slc2a6	4.4	0.144	0.6	0.668	1.7	1.000	0.2	0.478
Slc2a7	1.0	1.000	1.0	1.000	1.0	1.000	1.0	1.000
Slc2a8	1.0	0.919	1.0	0.970	0.9	1.000	1.0	0.998
Slc2a9	0.7	0.404	0.8	0.550	0.9	1.000	1.0	1.000
Slc30a1	1.3	0.505	1.6	0.051	1.0	1.000	1.3	0.799
Slc30a10	1.7	0.622	1.3	0.854	1.1	1.000	0.8	0.984
Slc30a2	2.0	0.661	2.1	0.775	0.3	1.000	0.3	0.747
Slc30a3	0.4	0.499	0.4	0.533	0.5	1.000	0.6	0.946
Slc30a4	1.4	0.351	1.4	0.333	1.1	1.000	1.1	0.985
Slc30a5	1.1	0.870	1.0	0.975	1.0	1.000	1.0	1.000
Slc30a6	1.2	0.552	1.2	0.454	1.0	1.000	1.0	1.000
Slc30a7	1.0	0.973	0.9	0.921	0.8	1.000	0.8	0.901
Slc30a9	0.8	0.245	0.8	0.181	1.0	1.000	1.0	1.000
Slc31a1	0.9	0.851	1.1	0.739	0.9	1.000	1.1	0.960
Slc31a2	1.1	0.797	1.1	0.751	0.9	1.000	0.9	0.971
Slc33a1	1.4	0.280	1.5	0.076	1.0	1.000	1.1	0.943
Slc34a2	2.6	0.176	2.0	0.403	0.6	1.000	0.5	0.694
Slc34a3	1.0	1.000	1.0	1.000	1.0	1.000	1.0	1.000
Slc35a1	0.9	0.827	1.1	0.578	0.8	0.999	1.0	1.000
Slc35a2	1.0	0.930	1.0	0.947	1.0	1.000	1.1	0.988
Slc35a3	1.0	0.937	1.1	0.709	1.0	1.000	1.1	0.978
Slc35a4	0.9	0.938	1.3	0.506	1.0	1.000	1.5	0.689
Slc35a5	1.1	0.800	1.0	1.000	1.1	1.000	1.0	1.000

Slc35b1	1.8	0.006	2.5	<0.001	1.0	1.000	1.3	0.617
Slc35b2	1.0	0.977	1.5	0.089	0.9	1.000	1.3	0.629
Slc35b3	1.1	0.771	1.3	0.272	0.8	1.000	1.0	0.996
Slc35b4	1.0	0.984	1.4	0.288	0.9	1.000	1.4	0.753
Slc35c1	1.3	0.254	1.6	0.029	0.9	1.000	1.1	0.953
Slc35c2	1.7	0.003	2.0	<0.001	0.9	1.000	1.0	1.000
Slc35d1	1.2	0.546	1.1	0.735	0.8	1.000	0.8	0.595
Slc35d2	1.2	0.542	1.5	0.131	0.8	1.000	1.0	1.000
Slc35d3	3.5	0.641	5.8	0.488	0.4	1.000	0.6	0.984
Slc35e1	1.1	0.628	1.0	0.919	1.1	1.000	1.0	0.997
Slc35e2	1.0	0.944	1.0	0.964	1.3	0.817	1.3	0.702
Slc35e3	0.8	0.483	0.7	0.158	0.9	1.000	0.8	0.745
Slc35e4	1.8	0.451	1.3	0.794	1.2	1.000	0.9	0.988
Slc35f1	1.8	0.798	0.8	0.937	1.7	1.000	0.7	0.994
Slc35f2	1.1	0.979	1.0	0.995	0.9	1.000	0.8	0.999
Slc35f3	1.0	1.000	2.3	0.532	0.8	1.000	1.8	0.917
Slc35f5	1.3	0.458	1.1	0.781	1.0	1.000	0.9	0.951
Slc35f6	1.0	0.942	1.1	0.876	1.0	1.000	1.1	0.971
Slc35g1	0.9	0.742	1.0	0.946	1.1	1.000	1.2	0.876
Slc35g2	0.7	0.754	0.7	0.684	1.6	1.000	1.5	0.865
Slc36a1	2.3	0.001	2.7	<0.001	0.9	1.000	1.0	1.000
Slc36a2	0.1	0.266	0.8	0.915	0.9	1.000	4.6	0.756
Slc36a4	1.1	0.901	1.2	0.598	0.9	1.000	1.0	1.000
Slc37a1	11.6	<0.001	6.2	<0.001	1.5	1.000	0.8	0.946
Slc37a2	1.2	0.832	0.7	0.424	0.8	1.000	0.5	0.350
Slc37a3	1.4	0.227	1.4	0.208	1.0	1.000	1.0	1.000
Slc37a4	0.5	0.094	0.6	0.135	1.3	1.000	1.4	0.809
Slc38a1	1.0	0.988	1.3	0.605	1.1	1.000	1.3	0.835
Slc38a10	1.3	0.351	1.6	0.062	0.8	1.000	1.0	1.000
Slc38a11	0.5	0.595	0.7	0.791	0.9	1.000	1.3	0.991
Slc38a2	1.1	0.704	1.3	0.202	1.4	0.322	1.6	0.107
Slc38a3	0.8	0.551	0.9	0.715	1.0	1.000	1.1	0.971
Slc38a4	0.3	<0.001	0.3	<0.001	1.1	1.000	1.2	0.951
Slc38a5	1.2	0.955	0.4	0.465	2.8	1.000	1.0	1.000
Slc38a6	0.9	0.914	0.9	0.751	1.1	1.000	1.0	1.000
Slc38a7	0.7	0.149	0.9	0.609	0.9	1.000	1.1	0.945
Slc38a8	1.2	0.967	0.9	0.958	3.3	1.000	2.5	0.865
Slc38a9	1.0	0.963	0.9	0.742	1.1	1.000	0.9	0.973
Slc39a1	1.0	0.998	1.2	0.507	0.9	1.000	1.1	0.965
Slc39a10	1.3	0.439	0.7	0.344	1.4	1.000	0.7	0.722
Slc39a11	1.4	0.180	2.0	<0.001	0.9	1.000	1.3	0.626
Slc39a13	1.1	0.728	1.1	0.853	1.0	1.000	1.0	1.000
Slc39a14	2.3	0.013	2.1	0.022	1.5	0.978	1.4	0.775
Slc39a2	0.6	0.522	0.5	0.208	1.1	1.000	0.9	0.988
Slc39a3	1.1	0.749	1.0	0.877	0.9	1.000	0.9	0.794
Slc39a4	0.9	0.817	0.7	0.358	0.8	1.000	0.6	0.603
Slc39a5	1.5	0.680	1.2	0.878	1.1	1.000	0.9	0.998
Slc39a6	1.0	0.990	1.0	1.000	1.3	1.000	1.3	0.843

Slc39a7	1.1	0.762	1.2	0.461	0.9	1.000	0.9	0.975
Slc39a8	1.0	0.996	1.1	0.817	1.0	1.000	1.2	0.949
Slc39a9	1.1	0.707	1.2	0.579	1.0	1.000	1.1	0.978
Slc3a1	1.0	1.000	1.8	0.469	0.7	1.000	1.2	0.985
Slc3a2	0.8	0.448	0.9	0.719	1.0	1.000	1.1	0.936
Slc40a1	1.5	0.292	1.6	0.180	0.7	1.000	0.8	0.837
Slc41a1	1.0	0.997	1.2	0.671	0.7	1.000	0.9	0.943
Slc41a2	30.2	<0.001	28.1	<0.001	1.1	1.000	1.0	1.000
Slc41a3	4.3	0.001	3.5	0.002	1.9	0.781	1.5	0.753
Slc43a1	2.6	0.037	3.1	0.010	1.1	1.000	1.3	0.934
Slc43a2	1.1	0.895	1.0	0.982	0.9	1.000	0.9	0.967
Slc43a3	0.8	0.493	0.8	0.334	1.0	1.000	0.9	0.962
Slc44a1	1.1	0.751	1.2	0.425	0.9	1.000	1.0	1.000
Slc44a2	0.9	0.721	0.8	0.477	1.0	1.000	0.9	0.943
Slc44a3	0.9	0.908	0.6	0.416	0.9	1.000	0.7	0.803
Slc44a4	0.6	0.844	2.6	0.389	1.6	1.000	6.9	0.404
Slc45a3	3.0	0.001	2.1	0.027	1.2	1.000	0.9	0.948
Slc45a4	1.2	0.706	1.4	0.343	0.7	1.000	0.8	0.912
Slc46a1	0.9	0.608	1.1	0.570	0.7	0.593	1.0	0.995
Slc46a3	0.5	0.090	0.9	0.866	0.7	1.000	1.4	0.844
Slc47a1	0.9	0.922	1.0	0.975	0.9	1.000	1.0	1.000
Slc48a1	1.1	0.749	1.0	1.000	1.0	1.000	0.9	0.914
Slc4a1	8.0	0.002	24.0	<0.001	0.9	1.000	2.6	0.415
Slc4a11	0.6	0.755	0.6	0.742	0.6	1.000	0.6	0.944
Slc4a1ap	0.8	0.268	0.7	0.074	1.0	1.000	0.9	0.869
Slc4a2	0.9	0.818	0.8	0.433	1.0	1.000	0.9	0.938
Slc4a3	0.6	0.469	0.9	0.856	0.9	1.000	1.3	0.930
Slc4a4	0.7	0.439	0.8	0.517	1.1	1.000	1.1	0.967
Slc4a5	1.3	0.926	0.3	0.436	2.9	1.000	0.6	0.984
Slc4a7	1.1	0.862	1.1	0.699	1.0	1.000	1.1	0.982
Slc4a8	1.1	0.978	0.3	0.272	0.9	1.000	0.3	0.557
Slc4a9	0.1	0.025	0.1	0.001	3.9	0.359	1.9	0.914
Slc50a1	0.6	0.144	0.8	0.703	0.9	1.000	1.3	0.816
Slc51a	0.3	0.381	0.3	0.424	0.4	1.000	0.4	0.795
Slc51b	1.4	0.835	0.9	0.943	0.8	1.000	0.5	0.820
Slc52a2	0.6	0.178	0.6	0.112	0.8	1.000	0.7	0.762
Slc52a3	0.9	0.931	1.6	0.605	1.1	1.000	2.0	0.762
Slc5a1	0.6	0.551	0.8	0.856	1.1	1.000	1.6	0.897
Slc5a11	0.5	0.758	0.5	0.734	0.4	1.000	0.3	0.868
Slc5a3	1.2	0.779	0.9	0.861	1.1	1.000	0.8	0.949
Slc5a4b	0.7	0.821	0.9	0.966	1.2	1.000	1.7	0.938
Slc5a5	1.8	0.786	2.1	0.703	0.6	1.000	0.7	0.999
Slc5a6	0.5	0.130	0.6	0.166	1.2	1.000	1.3	0.912
Slc5a9	8.5	0.247	0.4	0.685	8.4	0.908	0.4	0.912
Slc6a1	2.1	0.629	0.9	0.971	0.7	1.000	0.3	0.739
Slc6a12	1.1	0.952	1.6	0.137	0.9	1.000	1.4	0.718
Slc6a13	0.8	0.699	0.9	0.818	0.9	1.000	1.0	1.000
Slc6a14	0.5	0.769	3.5	0.348	0.8	1.000	5.4	0.575

Slc6a15	0.5	0.809	1.1	0.997	0.5	1.000	1.2	1.000
Slc6a16	0.3	0.253	0.4	0.249	1.4	1.000	1.5	0.941
Slc6a17	0.9	0.993	0.6	0.731	2.4	1.000	1.5	0.978
Slc6a18	2.9	0.637	7.4	0.293	1.0	1.000	2.6	0.901
Slc6a19	0.1	0.369	0.2	0.320	1.6	1.000	2.0	0.975
Slc6a2	4.6	0.452	0.9	0.953	6.0	0.979	1.1	1.000
Slc6a20b	1.6	0.646	0.6	0.525	1.5	1.000	0.6	0.799
Slc6a4	1.8	0.513	1.4	0.783	0.6	1.000	0.5	0.744
Slc6a6	1.2	0.713	1.6	0.159	0.8	1.000	1.0	1.000
Slc6a8	0.9	0.836	1.3	0.616	0.9	1.000	1.4	0.856
Slc6a9	6.1	<0.001	9.0	<0.001	0.7	1.000	1.1	1.000
Slc7a1	1.4	0.606	1.1	0.915	1.6	1.000	1.2	0.956
Slc7a10	0.3	0.619	0.4	0.559	2.8	1.000	4.4	0.763
Slc7a11	2.0	0.478	1.2	0.861	2.2	1.000	1.4	0.950
Slc7a14	0.6	0.680	0.3	0.273	1.5	1.000	0.7	0.978
Slc7a15	5.0	0.102	19.1	0.010	0.1	0.554	0.4	0.786
Slc7a2	0.4	0.013	0.5	0.058	1.3	1.000	1.6	0.625
Slc7a3	1.8	0.779	0.6	0.776	2.5	1.000	0.8	1.000
Slc7a4	1.1	0.933	1.0	1.000	0.9	1.000	0.8	0.971
Slc7a5	0.8	0.833	0.9	0.848	1.1	1.000	1.2	0.969
Slc7a6	0.5	0.451	2.3	0.214	1.0	1.000	4.6	0.262
Slc7a6os	0.9	0.658	0.8	0.243	1.0	1.000	0.9	0.947
Slc7a7	5.0	<0.001	2.9	0.003	1.1	1.000	0.6	0.601
Slc7a8	1.6	0.380	1.3	0.649	0.9	1.000	0.7	0.841
Slc7a9	8.0	0.255	14.3	0.138	0.6	1.000	1.1	1.000
Slc8a1	3.1	0.236	2.1	0.486	0.7	1.000	0.5	0.803
Slc8b1	0.5	0.023	0.6	0.055	0.8	1.000	0.9	0.958
Slc9a1	0.9	0.792	0.8	0.421	1.1	1.000	1.0	1.000
Slc9a2	0.8	0.965	13.0	0.056	0.3	1.000	4.9	0.575
Slc9a3	0.4	0.766	74.3	0.005	0.1	1.000	23.5	0.238
Slc9a3r1	0.6	0.055	0.7	0.229	0.9	1.000	1.1	0.951
Slc9a3r2	0.6	0.067	0.6	0.102	0.9	1.000	1.0	1.000
Slc9a5	1.0	0.998	0.7	0.518	1.2	1.000	0.8	0.951
Slc9a6	1.1	0.872	1.0	1.000	1.0	1.000	0.9	0.997
Slc9a7	1.7	0.429	2.3	0.141	0.6	1.000	0.9	0.979
Slc9a8	0.7	0.197	0.8	0.267	0.9	1.000	0.9	0.943
Slc9a9	1.3	0.567	1.1	0.861	0.9	1.000	0.8	0.855
Slc9b1	3.2	0.335	5.5	0.152	0.5	1.000	0.8	1.000
Slc9b2	1.3	0.734	1.2	0.795	1.1	1.000	1.0	1.000
Slco1a1	1.6	0.585	2.0	0.319	0.5	1.000	0.6	0.856
Slco1a4	0.4	0.045	0.4	0.063	1.1	1.000	1.2	0.945
Slco1a6	3.9	0.339	5.1	0.192	0.9	1.000	1.2	1.000
Slco1b2	0.5	0.316	0.6	0.375	1.1	1.000	1.2	0.964
Slco2a1	1.1	0.883	1.3	0.562	0.9	1.000	1.0	1.000
Slco2b1	0.9	0.806	1.1	0.859	1.0	1.000	1.2	0.869
Slco3a1	1.0	0.983	0.8	0.635	1.0	1.000	0.8	0.894
Slco4a1	0.5	0.475	0.6	0.524	1.1	1.000	1.3	0.976
Slco4c1	4.8	0.519	17.8	0.035	2.6	1.000	9.6	0.376

Slco5a1	1.8	0.479	0.3	0.180	2.1	0.982	0.4	0.636

Supplemental Table S3. Plasma concentrations of bile acids in CVNP, CVP, GFNP, and GFP female C57BL/6 mice. Data shown are means ± SD of 5-6 mice.

Bile Acids	Plasma Concentration (ng/ml)			
	CVNP	CVP	GFNP	GFP
Primary Bile Acids				
α-MCA	108.2 ± 78.4	714.2 ± 880.9	13 ± 17.7	7.7 ± 7.8
T-α-MCA	25.6 ± 4.4	465.7 ± 850.9	3550.7 ± 6505.9	998.5 ± 1451.9
β-MCA	340.5 ± 379.4	1112.7 ± 844.1	140.8 ± 175.5	65.7 ± 53.3
T-β-MCA	36.7 ± 17.7	2674.4 ± 5832.7	22884.7 ± 31772.6	9222.2 ± 10750
CA	393 ± 269.8	5678.6 ± 7628.4	49.6 ± 22.2	37.3 ± 4
CDCA	148.4 ± 36.3	892.2 ± 921.5	128.8 ± 52.1	100 ± 4.7
TCA	173.5 ± 85.8	2483.7 ± 4355.4	9636.8 ± 15368.9	3312 ± 5091.4
TCDCA	15.2 ± 5.5	60.5 ± 85.4	1081.5 ± 2185.7	244.4 ± 378.9
UDCA	68.2 ± 52	688.7 ± 762	3.3 ± 6	1.8 ± 2.3
TUDCA	14.7 ± 4.4	81.5 ± 149.2	797.1 ± 1651.7	268.3 ± 487
Secondary Bile Acids				
ω-MCA	351.5 ± 293.7	2101 ± 1967	0.1 ± 0	0.1 ± 0
T-ω-MCA	334.6 ± 104.4	2897.7 ± 5149.8	0.1 ± 0	0.1 ± 0
DCA	70.9 ± 69.7	478.1 ± 440.4	3.6 ± 7.3	6.3 ± 13.8
TDCA	46.2 ± 31.5	38 ± 16.6	1.7 ± 0	1.7 ± 0
MDCA	47.5 ± 4.2	80 ± 41	43.7 ± 0.6	43.5 ± 0.6
HDCA	225.8 ± 54.9	2037.8 ± 1492.2	29 ± 24.1	8 ± 6.1
THDCA	27.2 ± 10.2	86 ± 89.8	64.9 ± 67.2	31.1 ± 29.3
LCA	81.9 ± 33.8	160 ± 119.4	10.4 ± 9.1	1.9 ± 4
TLCA	19 ± 21.6	94.1 ± 117.3	8.3 ± 20.1	0.1 ± 0

Supplemental Table S4. Plasma concentrations of steroid hormones in CVNP, CVP, GFNP, and GFP female C57BL/6 mice. Data shown are means ± SD of 5-6 mice.

Steroid Hormones	Plasma Concentration (ng/ml)			
	CVNP	CVP	GFNP	GFP
11-deoxycorticosterone	43.5 ± 10.5	197.7 ± 100	107.8 ± 45.4	396.2 ± 112.7
17-OH-pregnenolone	621 ± 211	3329.6 ± 1731.1	910.1 ± 247.4	6186.2 ± 1770.4
17-OH-progesterone	43.4 ± 11.5	198.4 ± 106.9	112.5 ± 37.8	419.9 ± 129.4
Aldosterone	0.1 ± 0	1.7 ± 2.7	0.7 ± 1.5	10.3 ± 3.5
Corticosterone	693.4 ± 214.1	4089 ± 2135.5	1201 ± 252.4	7562.3 ± 2327.3
Cortisol	46.1 ± 19.7	1247.6 ± 741.7	80.8 ± 34.3	1749 ± 427.5
Cortisone	0.1 ± 0	6 ± 5.8	0.1 ± 0	7.4 ± 3.5
DHEA	2.3 ± 2.8	1.3 ± 1.3	0.3 ± 0.3	0.1 ± 0
Estradiol	67.8 ± 37.1	30.9 ± 10.1	65.3 ± 66.2	124.5 ± 128
Estrone	23 ± 19.2	8.6 ± 10.4	28.9 ± 53	20.4 ± 20.8
Pregnenolone	0.1 ± 0	2.5 ± 4.5	1.4 ± 2.4	6.7 ± 4.8
Progesterone	18.6 ± 15.7	577.2 ± 235.8	28.7 ± 47.3	458.5 ± 192.3
Testosterone	0.1 ± 0	0.1 ± 0	0.1 ± 0	0.1 ± 0